CYCLONE STRUCTURAL TESTING STATION
JAMES COOK UNIVERSITY OF NORTH QUEENSLAND

FULL-SCALE AND MODEL-SCALE WIND PRESSURE AND FATIGUE LOADING ON THE TEXAS TECH UNIVERSITY BUILDING

by

Y. L. Xu
and
G. F. Reardon

TECHNICAL REPORT NO. 42

August 1996

Xu, Y. L. (You Lin), 1952-
Full-scale and model-scale wind pressure and fatigue loading on the Texas Tech University building.

Bibliography.
ISBN 0 86443 605 X
ISSN 0158 - 8338.

1. Wind-pressure - Testing. 2. Buildings - Aerodynamics - Testing. 3. Materials - Fatigue - Measurement. I. James Cook University of North Queensland, Cyclone Structural Testing Station. II Title. (Series: Technical Report (James Cook University of North Queensland, Cyclone Structural Testing Station) ; no 42).

624.176

CONTENTS

Full-Scale and Model-Scale Wind Pressure and Fatigue Loading on the Texas Tech University Building*

Synopsis

The Texas Tech University Building is a well-instrumented, full-scale experimental building designed specially for the study of wind loads on low-rise buildings. It provides high quality full-scale data to check wind tunnel test results which have been included in wind loading codes in many countries. The systematic wind tunnel study on wind-induced fatigue loading is under way at the Cyclone Testing Station, requiring a comparison of fatigue loading at full scale and model scale. Therefore, a Texas Tech University Building model was made and tested at the James Cook University Boundary Layer Wind Tunnel to compare model-scale and full-scale wind pressures and fatigue loading in terms of pressure coefficient, pressure spectrum, probability distribution and extreme value distribution of wind pressures, the number of cycles, and cycle histogram.

Most wind pressure coefficients measured on the model were found to be in close agreement with full-scale wind pressure coefficients, but the largest negative peak coefficients at the roof edge and corners were underestimated by the wind tunnel tests. The consistency and disparity of full-scale and model-scale data also appeared in wind pressure spectrum, probability distribution, and extreme value distribution. A reasonable agreement of the number of cycles and cycle histograms at model-scale and full-scale was achieved when sampling frequency, sampling duration and particularly cut-off frequency used in wind tunnel tests were equivalent to those used in full-scale measurements.

The results from this study indicate that wind tunnel techniques can be used as an economic and efficient way to determine wind pressures and fatigue loading on low-rise buildings, but caution should be given to the largest negative peak pressures at roof edge and corners.

---

* A summary version of this report has been published in Proceedings of the Second International Workshop on Full Scale Behaviour of Low Rise Buildings, Townsville, Australia, 1994

1 INTRODUCTION

Static and dynamic wind pressures on houses and low-rise buildings have been extensively investigated through wind tunnel tests in the past two decades. The test results have also been widely incorporated in wind loading codes in many countries (Holmes, 1980; Stathopoulos, 1984). Relatively few comparisons however have been made between full-scale and model-scale test data. This is due to limited full-scale measurements and the quality of full-scale data.

A research facility consisting of a test building and a meteorological tower has been recently constructed in the field at Wind Engineering Research Field Laboratory (WERFL) of the Texas Tech University, USA (Fig. 1). This facility combines the best features of the past full-scale facilities with advanced instrumentation and computer technology, aiming to provide high quality data to check wind loads from wind tunnel tests as well as newly developing computational fluid dynamics technology.

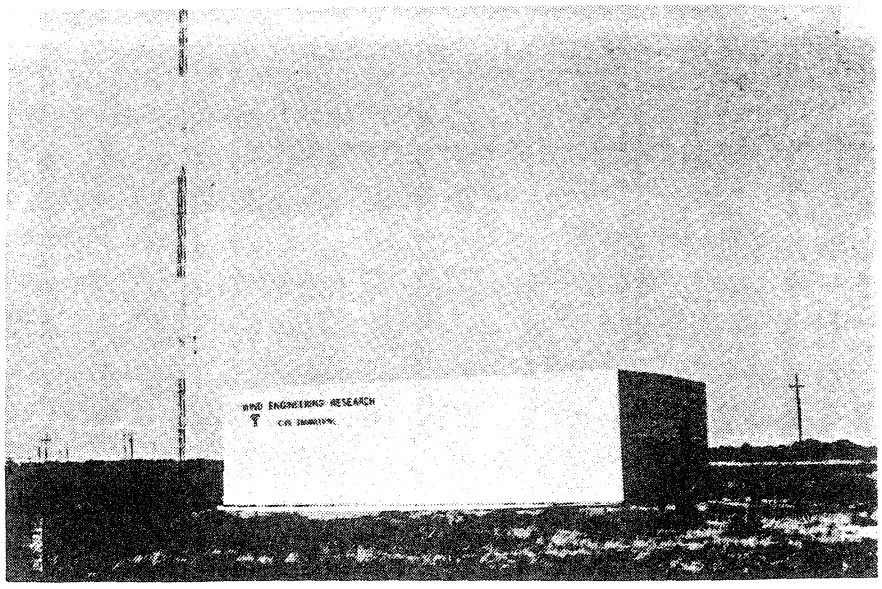

FIG.1 TEXAS TECH UNIVERSITY EXPERIMENTAL BUILDING

While static and dynamic wind loads on low-rise buildings have been extensively investigated before, wind-induced fatigue loading has not been

thoroughly explored to date. A number of post disaster investigations already showed that strong winds could cause severe fatigue damage to light gauge steel roof claddings (Walker, 1975; Smith, 1993). A great deal of research should be devoted to this area. As there exists a variety of building configurations and wind environments in the world, using wind tunnel model test techniques to determine or codify fatigue loading is therefore inevitable However, before an extensive wind tunnel investigation can be conducted, a careful comparison of fatigue loading at model scale and full scale is imperative.

To the purposes described above, a 1:50 scale model of the Texas Tech University Building was built and tested in the James Cook University Boundary Layer Wind Tunnel with a properly simulated wind environment. The wind pressures and fatigue loading obtained from the model tests were compared with the full-scale results.

2 EXPERIMENTAL TECHNIQUE

2.1 Texas Tech University Building

The Texas Tech University Building (TTU building) is a 9.1 x 13.7 x 4.0 m flat roof metal building located in an open terrain. A number of pressure taps of 9.5 mm internal diameter are arranged on the surface of the building. Pressure transducers connected to pressure taps convert air pressures into electrical signals, which are sent to a data acquisition system controlled by a microcomputer. The TTU building can be rotated, permitting positive control over wind angle of attack. The 49 m high meteorological tower is equipped with anemometers and vanes used to collect information on wind speed and wind direction. In the centre of the TTU building there is a concrete block room housing the data acquisition system. Further information on this facility can be found in Levitan and Mehta (1992a, 1992b) and Yeatts and Mehta (1994).

2.2 Building Model and Wind Tunnel

The TTU building model was made from "perspex" at a geometric scale of 1:50. The model configuration and pressure tap locations are schematically shown in Fig. 2. The 0^0 wind direction defined here is the same as that used by WERFL in full-scale tests, but it is different from the Australian Wind Loading Code (SAA, 1989). The pressure taps were located at positions scaled to those used in the full-scale building. The taps were

made from short-length, stainless-steel, hypodermic tubing of 1 mm internal diameter.

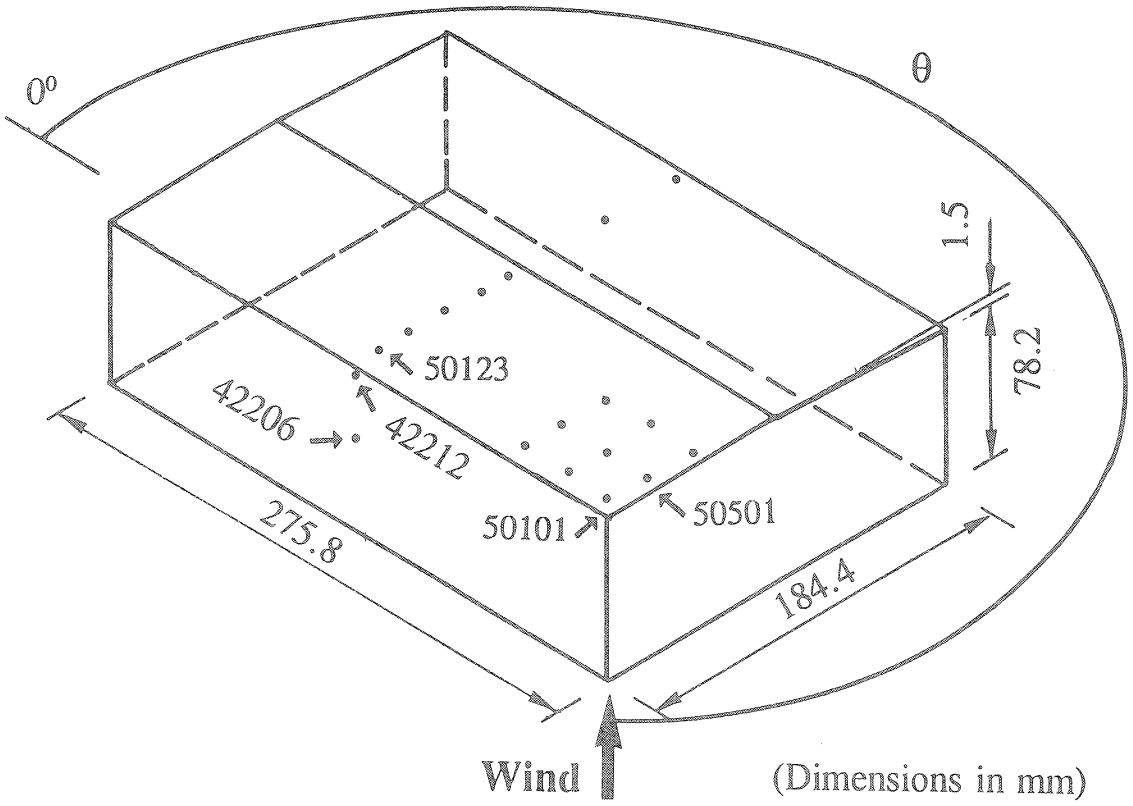

FIG.2 MODEL CONFIGURATION AND PRESSURE TAP LOCATIONS OF TTU BUILDING - WIND AT 225°

Model tests were carried out in the James Cook University Boundary Layer Wind Tunnel. It is an open-circuit suction wind tunnel with a working section of 17.5 x 2.5 x 2.1 m (Fig. 3). The model was mounted at the centre of the turntable, which allows the model to be tested at any wind direction. Further information on the wind tunnel can be found in Holmes (1980).

2.3 Flow Simulation

A 1:50 scale model of natural wind flow in open terrain was developed in the wind tunnel to simulate the natural wind on the field site of the TTU building. The flow simulation technique mainly consisted of mounting a 400 mm high single plain fence spanning the floor at the start of the test section

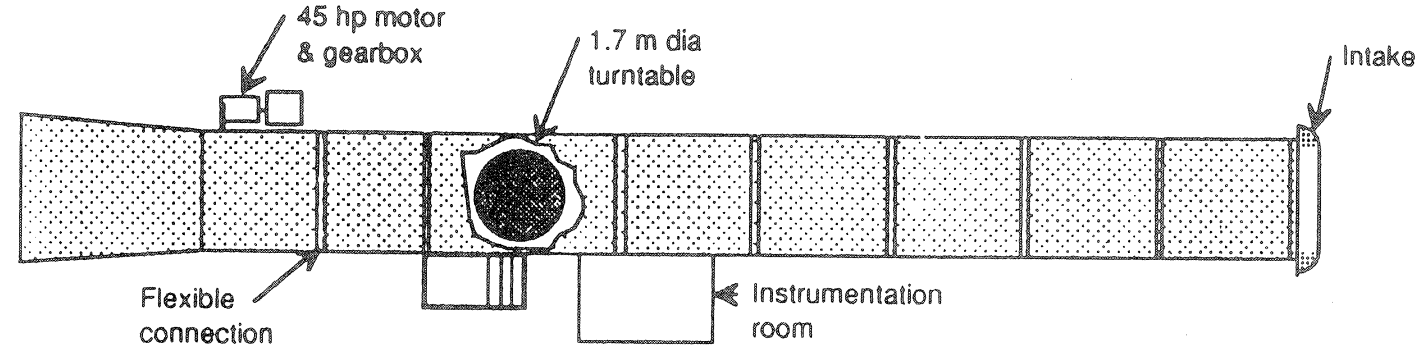

PLAN

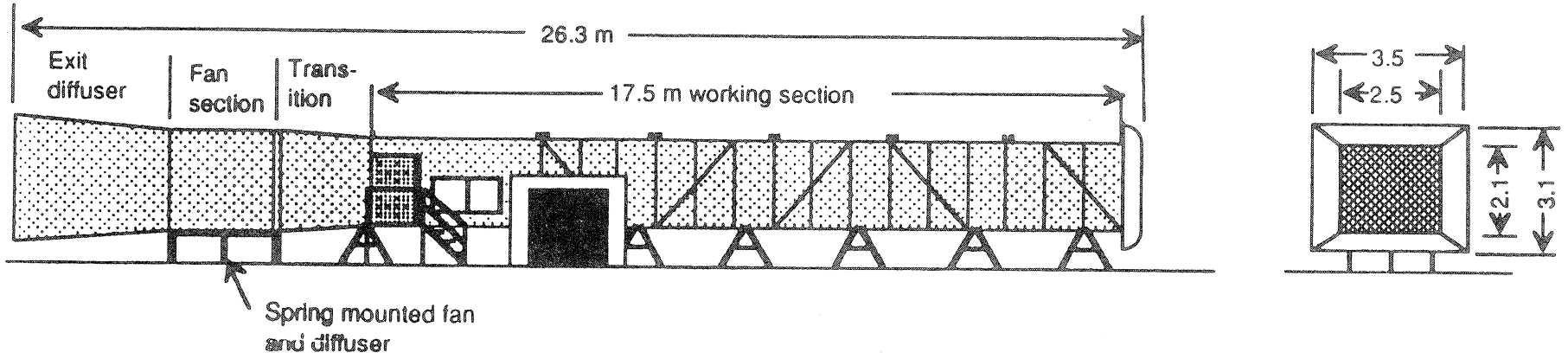

ELEVATION

FIG.3 JAMES COOK UNIVERSITY'S BOUNDARY LAYER WIND TUNNEL

and covering the whole working section with low-pile carpet. Wind velocity was measured using a hot film probe in conjunction with a constant temperature linearised anemometer.

Fig. 4 shows the mean longitudinal wind velocity profile measured at the centre of the turntable together with the empirical profiles from a logarithmic law and a power law. A power-law exponent α of 0.14 represents a mean value of α for a set of 24 profiles measured in the field of the TTU building (Cermak and Cochran, 1992). A logarithmic law with a roughness length z_0 of 0.02 m (full scale) corresponds to an open terrain. The reference height z_r of 10 m (full scale) is used in Fig. 4. It is clear that the mean longitudinal wind velocity profile in the wind tunnel is in good agreement with the mean longitudinal wind velocity profile in the field site of the TTU building.

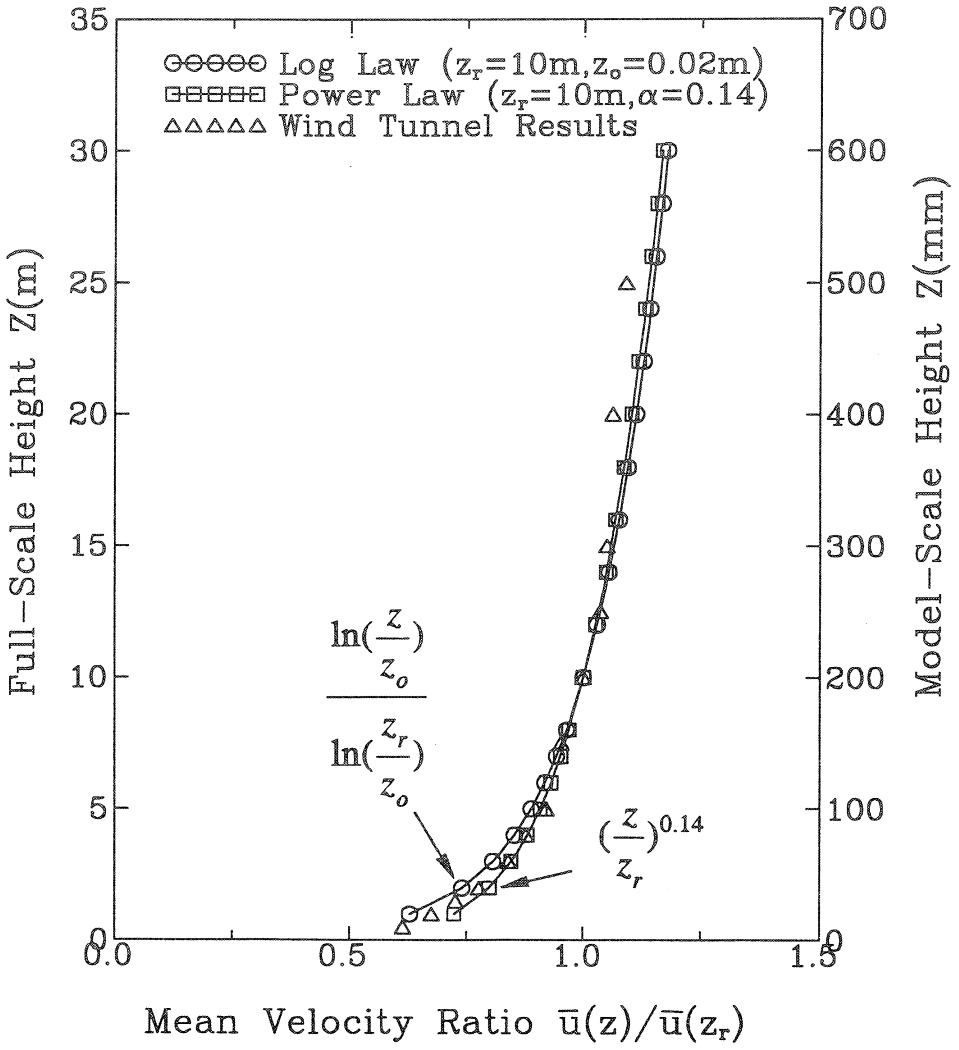

FIG.4 MEAN WIND VELOCITY PROFILES

Plotted in Fig. 5 are the longitudinal turbulence intensity profiles. The

model turbulence intensities above a full-scale height of 5 m are larger than those predicted by both logarithmic and power laws, but they are close enough to the mean values of field turbulence intensities. Below 5 m the turbulence intensities in the wind tunnel are larger than the mean value of field turbulence intensities, but they are in good agreement with the values predicted by the logarithmic law. The mean velocity at the eaves height of the model is about 10.5 m/s and the turbulence intensity at this height is about 0.2. The gradient height used in Fig. 5 is 300 m in full scale.

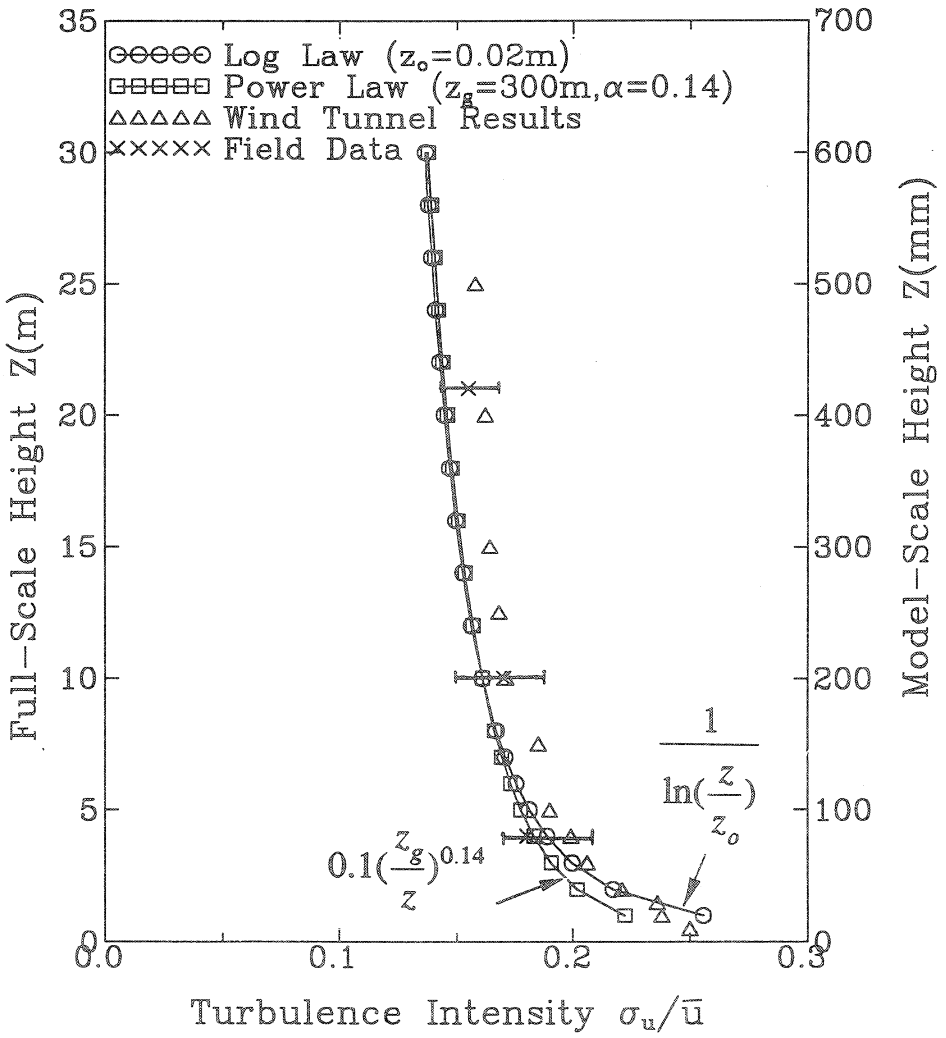

FIG.5 LONGITUDINAL TURBULENCE INTENSITY PROFILES

Model-scale and full-scale normalised longitudinal turbulence spectra at the eaves height are given in Fig. 6 together with the Karman spectrum of 51 m integral length, l_{ux}. The full-scale mean wind velocity at the eaves height is 10.1 m/s, close to the mean wind velocity at the eaves height in the wind tunnel. In lower frequency region ($n/\bar{u}$ less than 0.1 in full scale), the full-

scale turbulence spectrum is in good agreement with the Karman spectrum, but in higher frequency region the amplitudes of the full-scale spectrum drop off rapidly. The model turbulence spectrum, on the other hand, has a slightly smaller integral length of about 42 m.

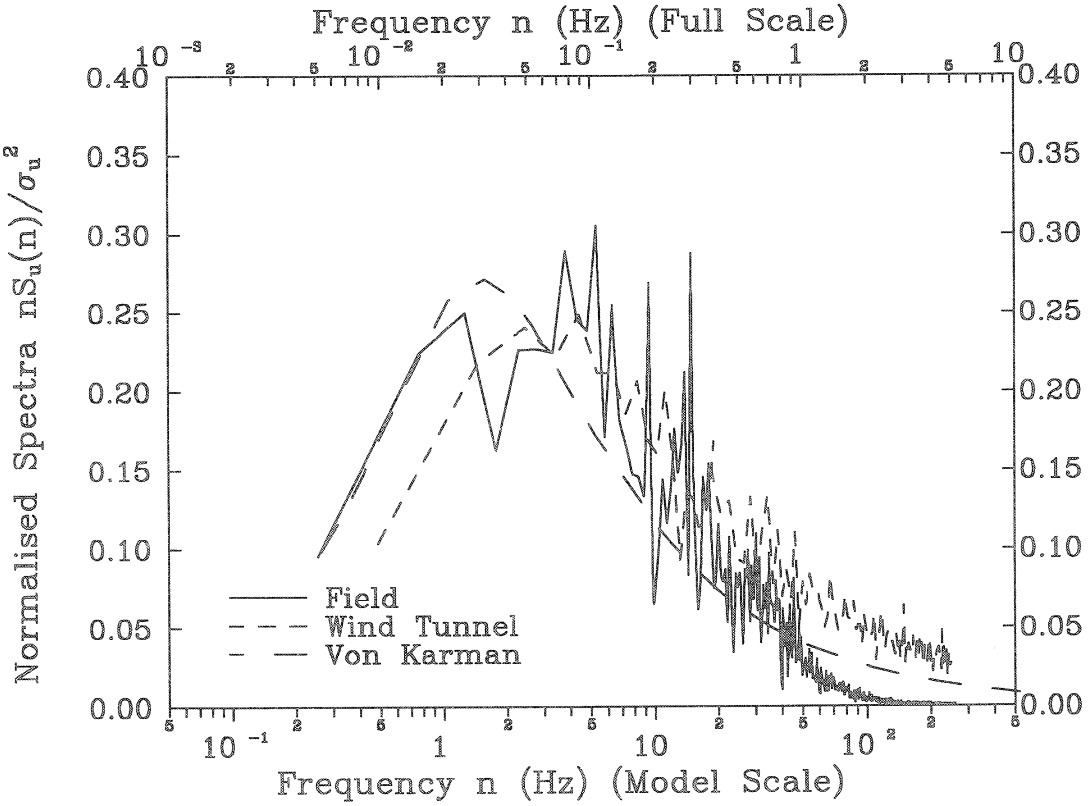

FIG.6 LONGITUDINAL TURBULENCE SPECTRA AT ROOF HEIGHT

Recently, Tieleman (1993) suggested to place small spires directly upstream from the test model with the purpose of improving the simulation of the lateral turbulence and the small scale turbulence in both longitudinal and lateral components. This simulation technique was not used in this study, but will be considered later.

2.4 Instrumentation and Measurement

The pressure taps on the building model were grouped and connected to two 48 port 'Scanivalves', which manipulate pressure measurements automatically. The connection between a tap and a scanivalve was a 450 mm length of p.v.c. tubing of 1.6 mm internal diameter and with two 0.3 mm internal diameter restrictors placed along the tubing. Mounted within the

scanivalves were two Honeywell 163 pressure transducers, converting air pressures into electrical signals. This measurement system had a linear frequency response up to 100 Hz and a gradual attenuation from 100 Hz to about 300 Hz with a 'half power' point.

The electrical signals from the transducers were low-pass filtered at 250 Hz via two electrical filters, and digitally sampled by a Data 6000 analyser at 1000 Hz for 32 seconds. Mean, root-mean-square (rms), minimum and maximum pressure coefficients were processed on line by a mini-computer. The reference velocity was taken on line at the eaves height of the model at a point about 200 mm upwind and 500 mm across wind from the model centre-lines. The wind velocity at the same scaled position as the field anemometer tower was also measured to provide a check on the reference velocity. The static pressure was taken from the static holes of a pitot tube mounted at 1 m above the tunnel floor and used for calibration of the hot film. In terms of a profile of static pressure through the boundary layer, a small correction could be made to convert the static pressure at the pitot tube to that at the eaves height or the floor surface.

At a length ratio of 1:50 and a velocity ratio of about 1, the sampling frequency and sampling length used in the wind tunnel tests were equivalent to about 20 Hz and 25 minutes in full scale. For some of the taps, the digital pressure data were stored in time history and were further analysed to obtain pressure spectra, probability and extreme value distributions, the number of cycles, and cycle histograms.

3 COMPARISON OF WIND PRESSURES

3.1 Pressure Coefficients

The statistical properties of wind pressures were specified by mean, rms, minimum and maximum pressure values in this study. These values were then normalised to non-dimensional coefficients using a dynamic pressure at the reference position. The definitions of these coefficients are as follows:
mean pressure coefficient,

$$\bar{C}_p = \frac{\bar{p} - p_o}{\frac{1}{2}\rho \bar{u}_r^2} \qquad (1)$$

rms pressure coefficient,

$$\acute{C}_p = \frac{\sqrt{\overline{(p(t)-\bar{p})^2}}}{\frac{1}{2}\rho \bar{u}_r^2} \tag{2}$$

minimum pressure coefficient,

$$\check{C}_p = \frac{\check{p}-p_o}{\frac{1}{2}\rho \bar{u}_r^2} \tag{3}$$

maximum pressure coefficient,

$$\hat{C}_p = \frac{\hat{p}-p_o}{\frac{1}{2}\rho \bar{u}_r^2} \tag{4}$$

where p(t) = the pressure; p_o = the static pressure at the eaves height; $\bar{u}_r$ = the mean velocity at the eaves height; and ρ = the air density. The minimum or maximum pressure coefficient is also called the largest negative or positive peak coefficient.

Presented in Fig. 7 are the pressure coefficient distributions over the central transverse section of the building for wind normal to the ridge line. Only the largest peak coefficients having the same sign as the mean pressure coefficients are plotted in Fig. 7. The full-scale data were provided by the WERFL with the following test specifications: the sampling frequency was 40 Hz; the sampling length was 15 minutes; the signals were low-pass filtered at 8 Hz; and the reference wind velocity was at the eaves height. Only one record for each tap was available, analysed to give the full-scale pressure coefficients. The model-scale data were an average of two records.

It can be seen from Fig. 7 that the mean and rms pressure coefficients from the wind tunnel tests are in good agreement with those from the full-scale measurements. The model-scale largest peak coefficients are however generally smaller than the full-scale largest peak coefficients. This discrepancy is partly because the full-scale cut-off frequency and sampling frequency are higher than those used in the wind tunnel tests. Surry (1991) also carried out a model-scale investigation on the TTU building using a wind tunnel of the University of Western Ontario. His results are nearly the

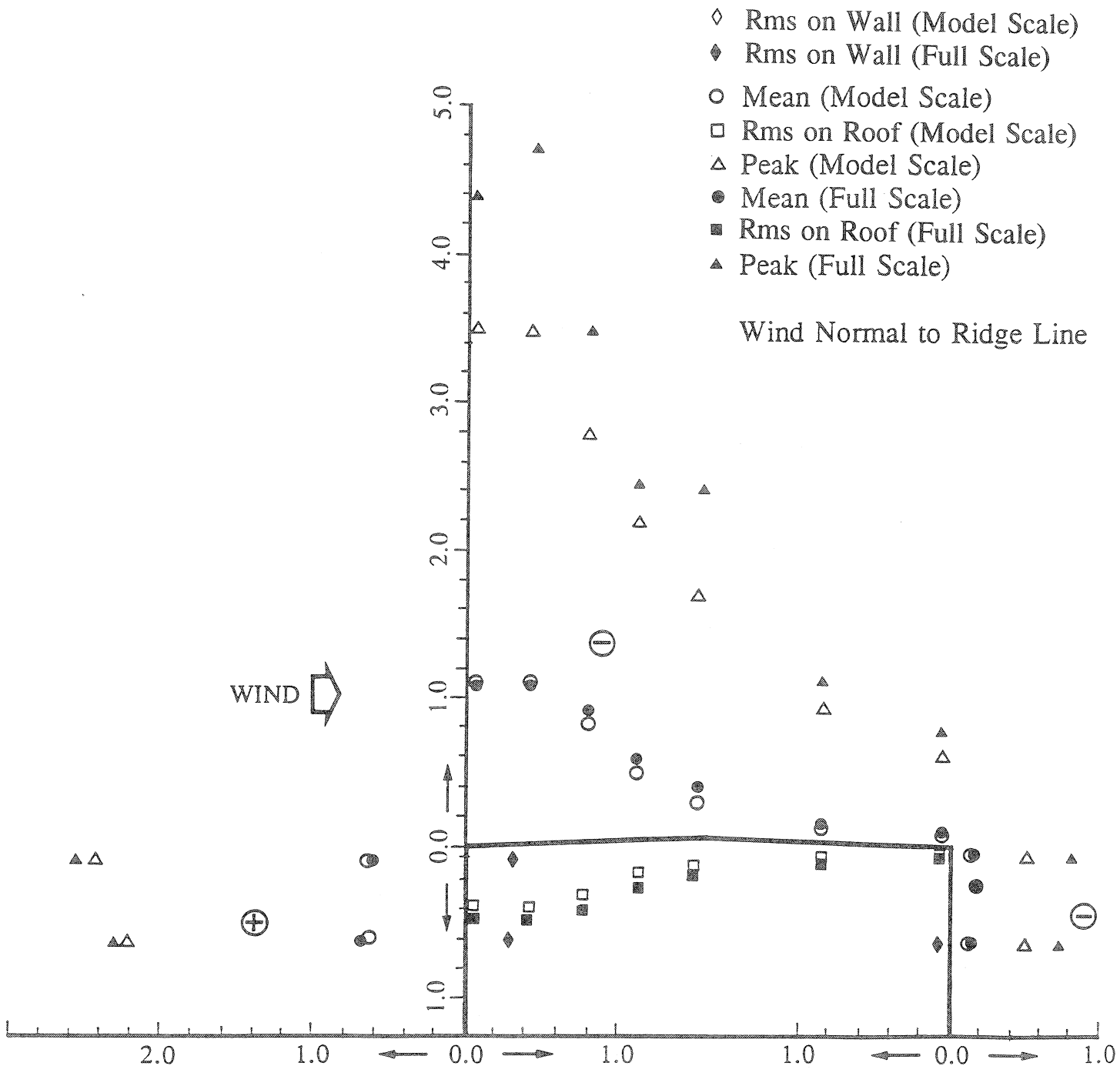

FIG.7 COMPARISON OF PRESSURE COEFFICIENTS ALONG CENTRAL TRANSVERSE SECTION OF BUILDING

same as the wind tunnel results obtained here.

Mehta et al (1992) presented the variation of the full-scale pressure coefficients at taps 50101, 50501, and 42206 with wind angle of attack. Cochran and Cermak (1992) published the model-scale pressure coefficients at the same taps on a 1:100 scale TTU building model. As seen in Fig. 2, taps 50101 and 50501 are at the roof corner along the edge. Tap 42206 is at the mid-height of the front wall at the central transverse section.

The variations of pressure coefficients with wind direction are shown in Fig. 8 to Fig. 10 for each of three taps at model scale and full scale. The results obtained here are found to be in good agreement with the wind tunnel results obtained by Cochran and Cermak (1992). They are also in close agreement with the full-scale results at most wind angles as shown in Fig. 8 to Fig. 10. The exception is the largest negative peak coefficients at taps 50101 and 50501 at the critical wind angles from 200^0 to 250^0. The model-scale largest negative peak coefficients are much smaller than the full-scale test results. The reason behind this is being discussed by many scholars (e.g. Tieleman, 1993). The following discussion on stochastic characteristics of wind pressure also aims to explain this disparity between model-scale and full-scale results.

3.2 Power Spectra

Power spectra of wind pressures can be used to identify pressure energy distribution in frequency domain. The cut-off frequency used in model and full-scale tests means to ignore wind pressure energy of higher frequency.

Figs. 11(a) to 11(d) show the model-scale and full-scale wind pressure spectra of taps 50101, 50501, 50123 and 42212 at their critical wind angle of attack. Tap 50123 is located at the roof edge at the central transverse section of the building (Fig. 2). Tap 42212 is located at the front wall at the central transverse section. The cut-off frequency used in the full-scale tests is 10 Hz for taps 50101 and 50501 and 8 Hz for taps 50123 and 42212. The cut-off frequency used in the wind tunnel tests is equivalent to 2 Hz for all the four taps. For taps 50101 and 50501, critical wind angle of attack is 225^0 in the model tests but it is only an approximation in the full-scale tests due to variation of wind direction in the field. For taps 50123 and 42212, critical wind angle of attack is 270^0 in the model tests (Fig. 2) and again it is only an approximation in the full-scale tests.

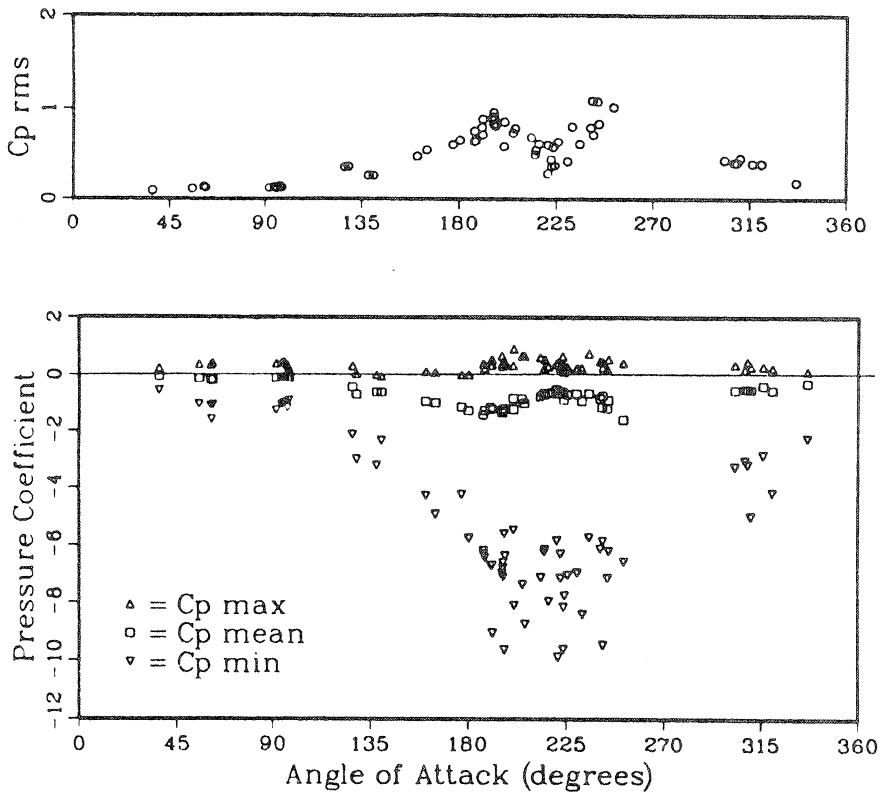

(a) Full Scale (Mehta et al)

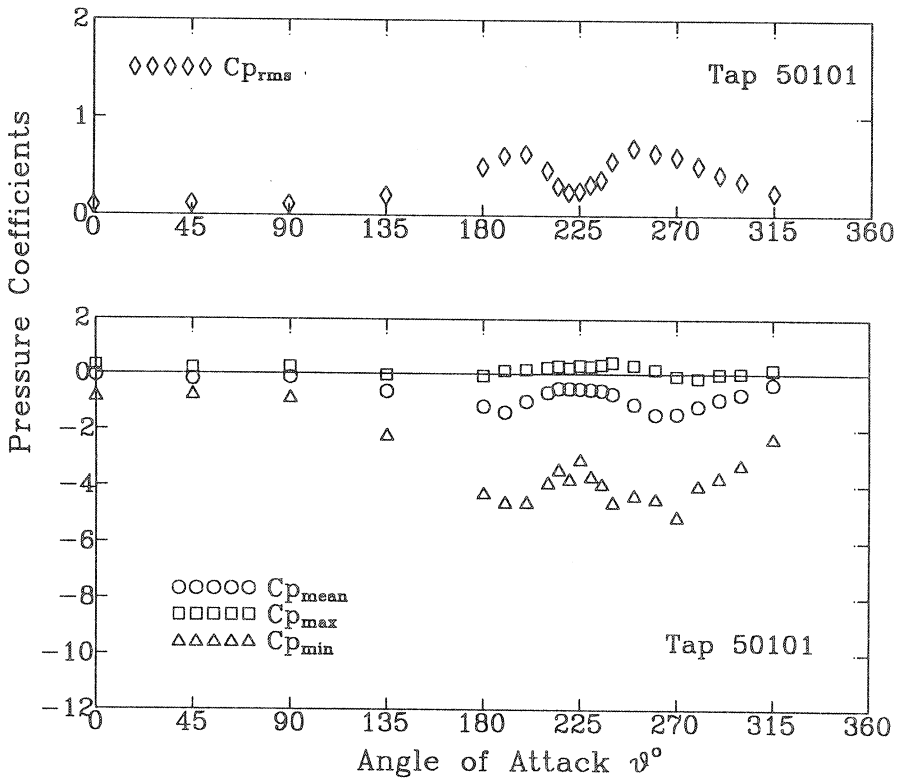

(b) Model Scale

FIG.8 VARIATION OF PRESSURE COEFFICIENTS WITH WIND ANGLE OF ATTACK (TAP 50101)

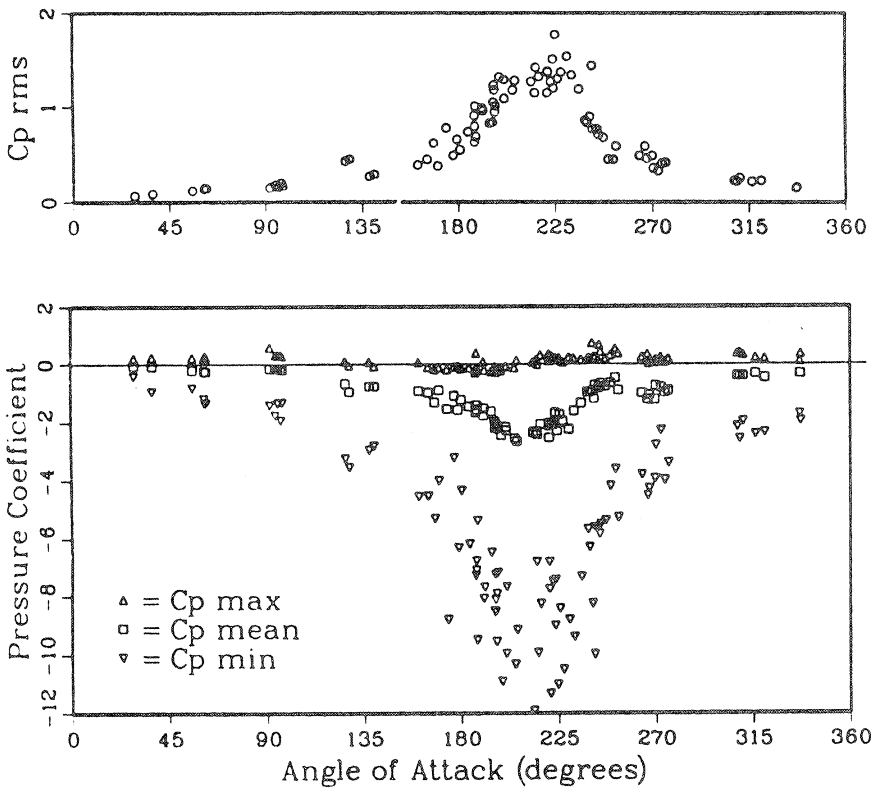

(a) Full Scale (Mehta et al)

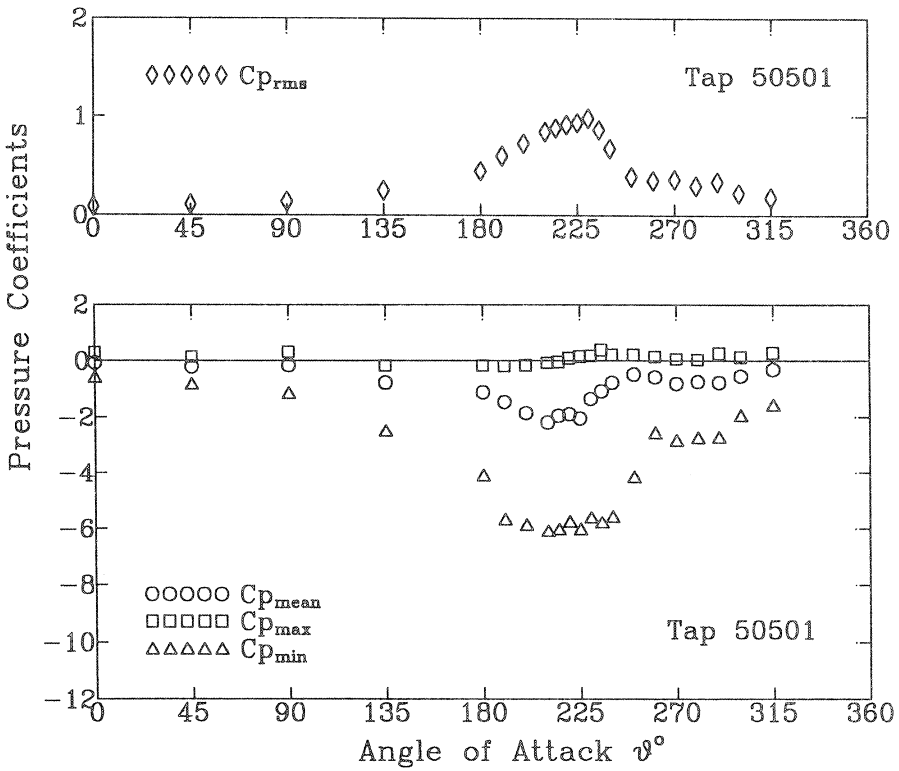

(b) Model Scale

FIG.9 VARIATION OF PRESSURE COEFFICIENTS WITH WIND ANGLE OF ATTACK (TAP 50501)

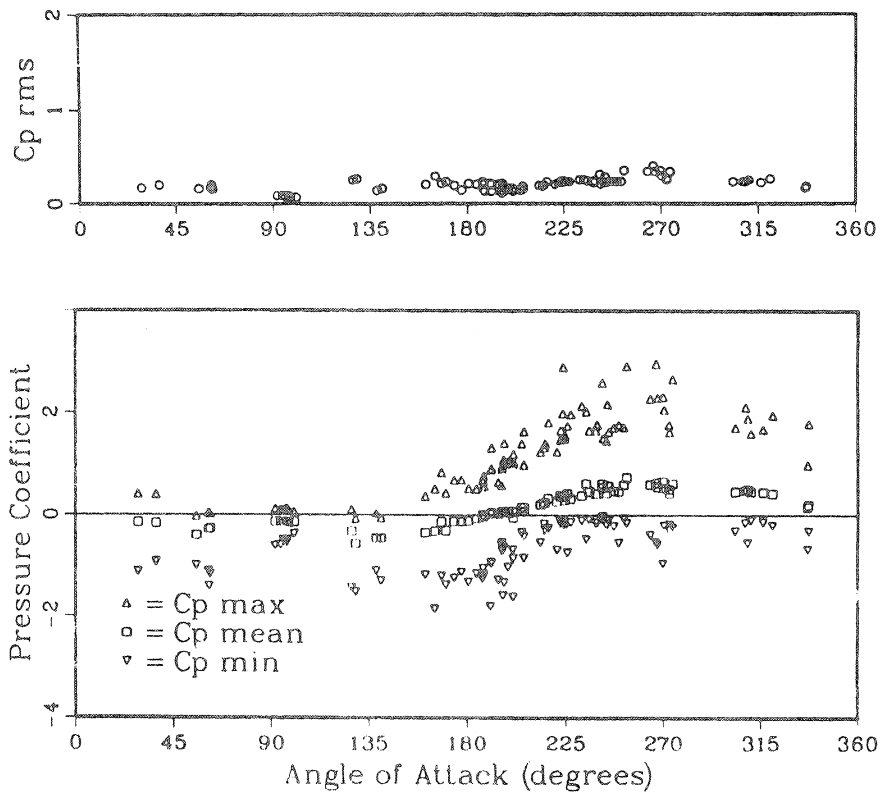

(a) Full Scale (Mehta et al)

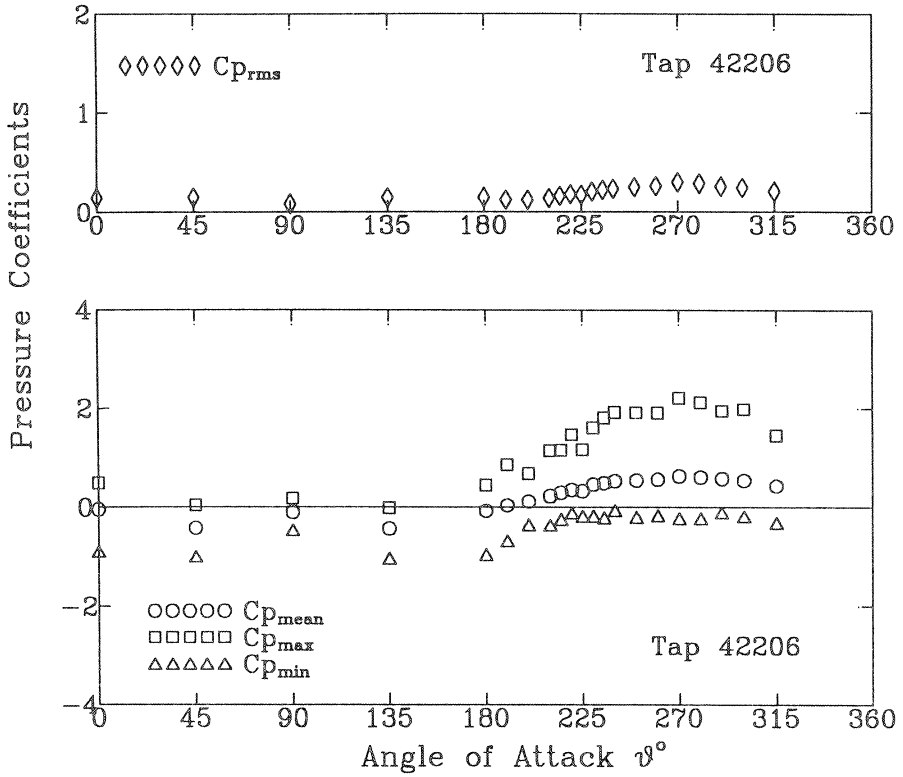

(b) Model Scale

FIG.10 VARIATION OF PRESSURE COEFFICIENTS WITH WIND ANGLE OF ATTACK (TAP 42206)

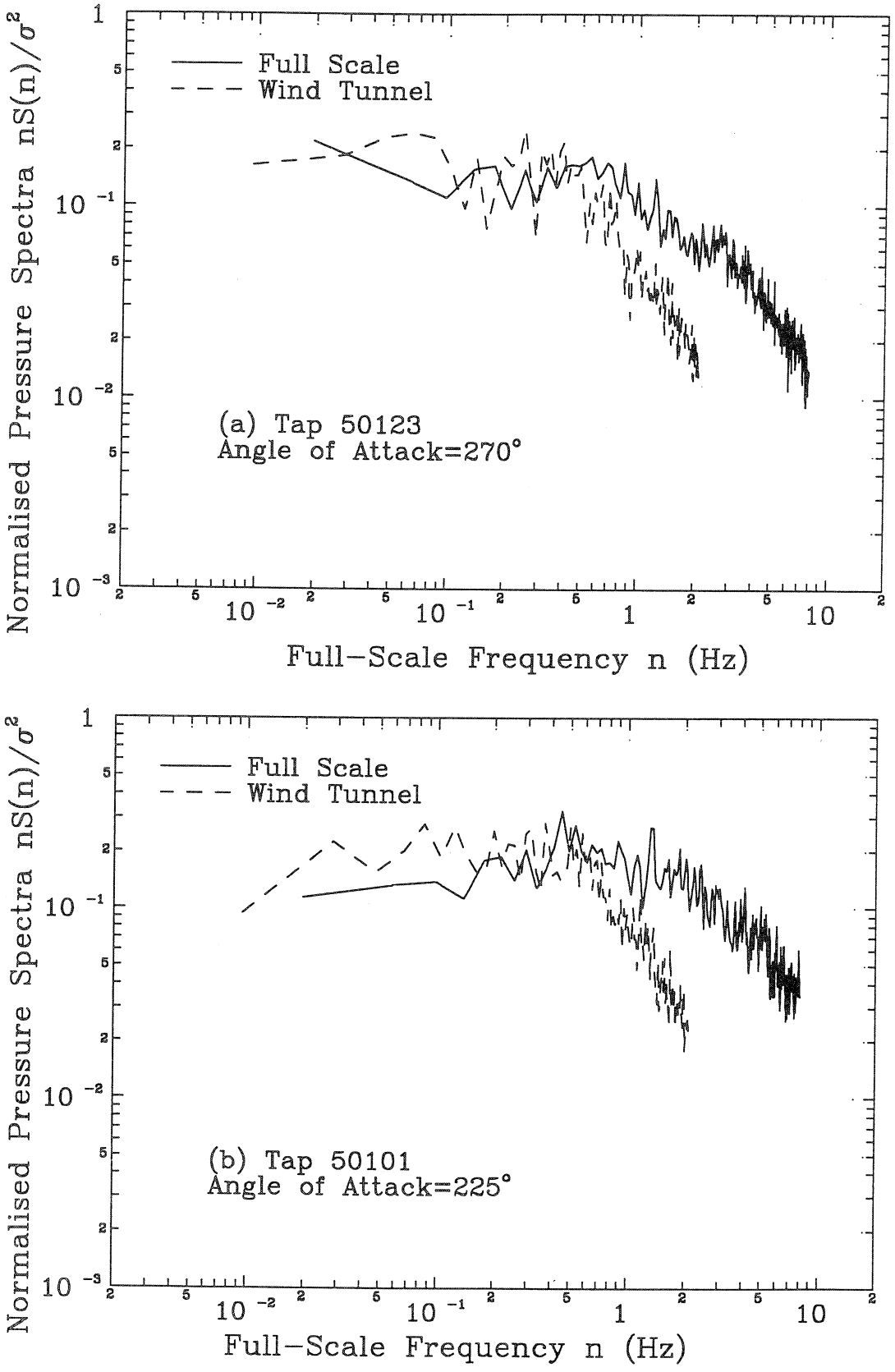

FIG.11 COMPARISON OF WIND PRESSURE SPECTRA

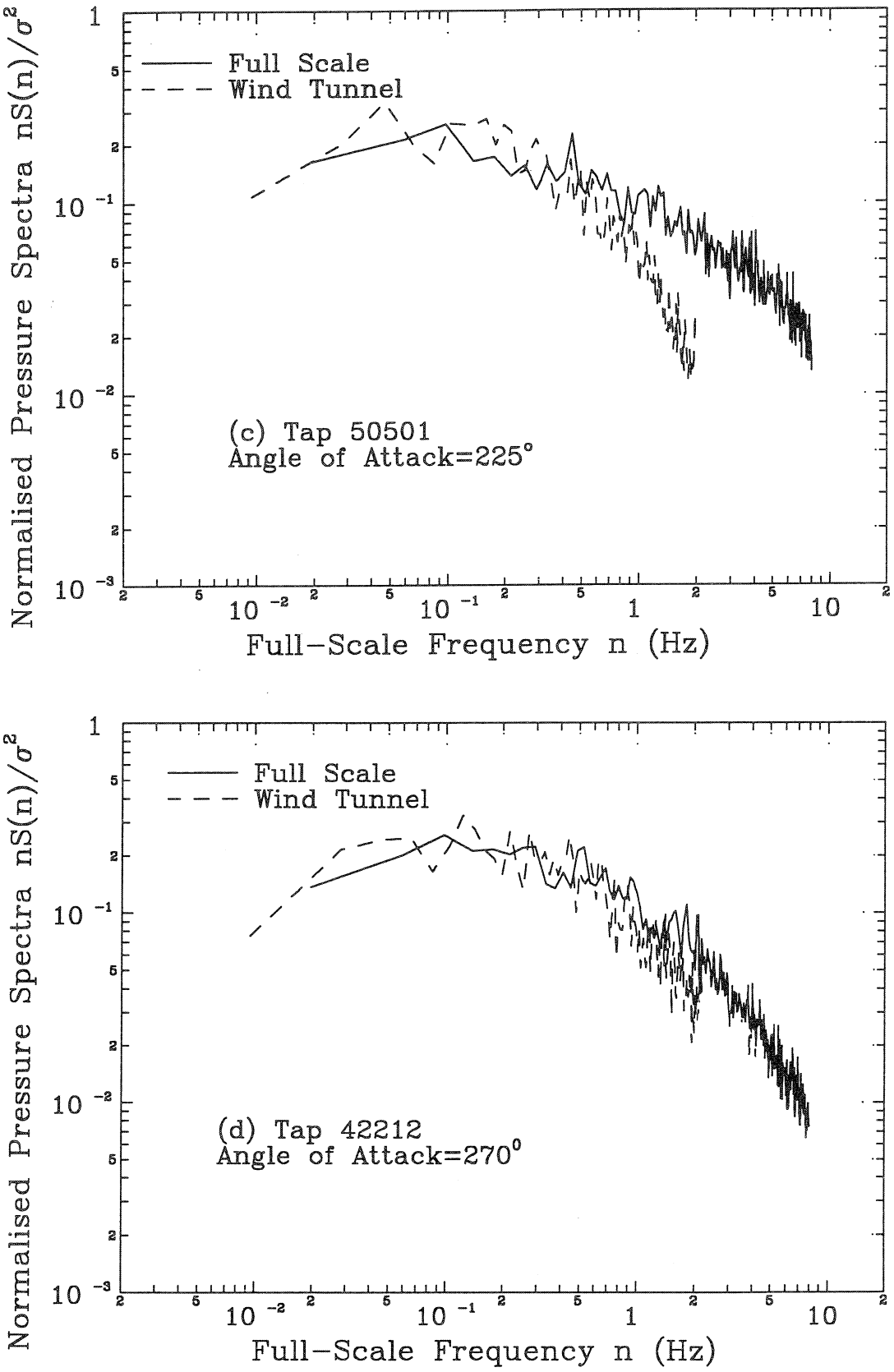

FIG.11 (continued) COMPARISON OF WIND PRESSURE SPECTRA

It can be seen from Figs. 11(a) to 11(d) that all the spectra are broad band, i.e., significant fluctuating energy distributes over a broad frequency range. The full-scale spectrum of tap 50501 is similar to the full-scale spectrum of tap 42212. The full-scale spectral amplitudes of tap 50123 in lower frequency range are less than those of tap 42212, but in higher frequency range two full-scale spectra are similar. The full-scale spectrum of tap 50101 shows a significant difference from that of tap 42212: the amplitudes of tap 50101 in higher frequency range are larger whilst the amplitudes in lower frequency range are smaller than those of tap 42212.

The model-scale spectrum of the wall pressure (tap 42212) is in good agreement with the full-scale spectrum of the same tap within the range below the cut-off frequency of 2 Hz. Compared with the full-scale spectra, the model-scale spectral amplitudes of all the roof pressures are lower in higher frequency range from 0.8 Hz to 2 Hz. This indicates that small scale turbulence caused by interaction of incident turbulence with the building local configuration around the roof taps in the field may be not appropriately simulated in the wind tunnel tests. The discrepancy of power spectra causes the discrepancy of the largest peak coefficients to some extent, as will be discussed later.

3.3 Probability Density Functions

Probability density function is one of stochastic characteristics of wind pressures, from which the severity of wind peak pressures can be estimated and the decision of choosing a suitable method to count load cycles of wind pressures can be made.

Probability density functions of wind pressures are usually expressed in peak factor form. The dimensionless peak factor, g(t), is defined as

$$g(t)=\frac{p(t)-\bar{p}}{\acute{p}}=\frac{C_p(t)-\bar{C}_p}{\acute{C}_p} \tag{5}$$

Fig. 12(a) shows the probability density functions of tap 50123 from both model-scale and full-scale tests together with the standard Gaussian density function. Obviously, the probability distribution of tap 50123 is not a Gaussian distribution. There are significant deviations from the Gaussian density function on both tails of the peak factor. As shown in the full-scale data, a significant number of data points are past five standard deviations

from the mean, which indicates a much higher probability for the larger negative peak pressures than a Gaussian density function would predict. On the other hand, the probability of the larger positive pressures are smaller than those predicted by a Gaussian density function. The peak of the function is also shifted slightly to the positive peak factor side, compared with the Gaussian density function. All of this evidence indicates that the pressure under cylindrical vortices is very negative. Similar observations were reported by Peterka and Cermak (1975) and Stathopoulos (1982). It is also seen from Fig. 12(a) that the probability density function obtained from the wind tunnel tests is similar to the full-scale function. This means that the probability nature of the strong negative pressures caused by cylindrical vortices is properly simulated by the wind tunnel tests though there is a discrepancy of the largest negative peaks between model scale and full-scale tests.

The most severe deviations from the Gaussian distribution can be observed in Fig. 12(b) for tap 50101. Both the model- and full-scale peak factors significantly deviate from the Gaussian density function on the negative side. The minimum peak factor is nearly -11. Observations of the pressure traces at this tap suggest that such distributions are attributed to a small number of isolated peaks of both short duration and high suction together with a large number of fluctuations of small suction around the mean.

Both the full- and model-scale probability density functions of the pressure fluctuation at tap 50501 do not significantly deviate from the Gaussian density function (Fig. 12(c)) though the location of tap 50501 is close to tap 50101. The reason behind this is probably that tap 50101 is located at the intersection of two "delta-wing" vortices along each windward edge whilst tap 50501 is under a single "delta-wing" vortex only.

The model- and full-scale probability density functions of tap 42212 on the front wall shown in Fig. 12(d) are in good agreement. Compared with the Gaussian density function, the pressure density functions in this case are shifted towards the positive peak factor side, a reversed situation of tap 50501. This also indicates why the spectrum of tap 42212 is similar to that of tap 50501.

In view of the preceding discussion, wind pressures concerned here do not follow a Gaussian distribution. The probability density functions from the wind tunnel tests were in good agreement with the full-scale data, which

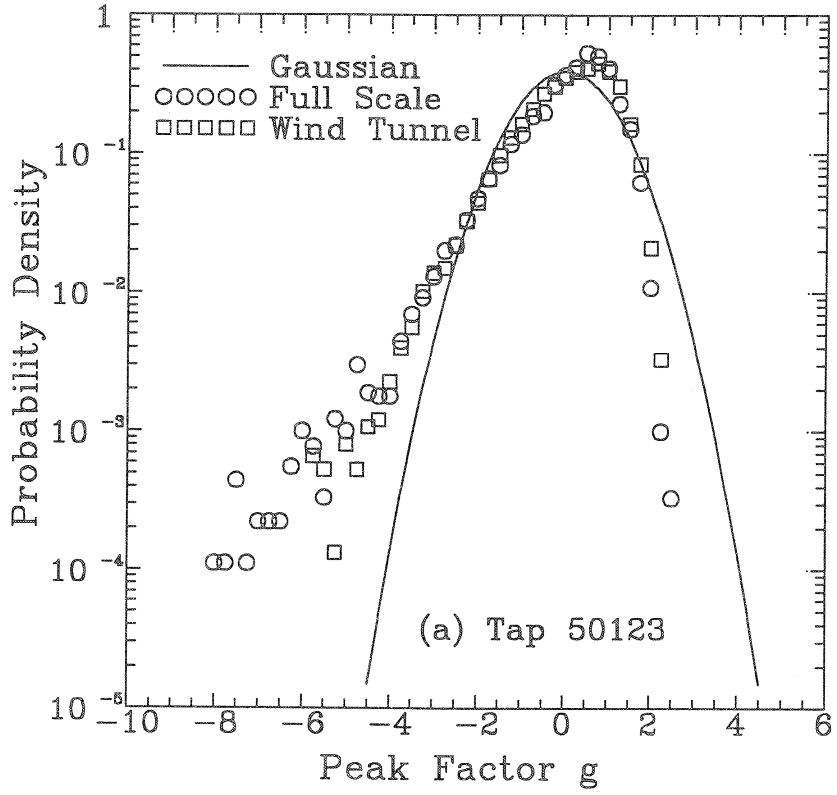

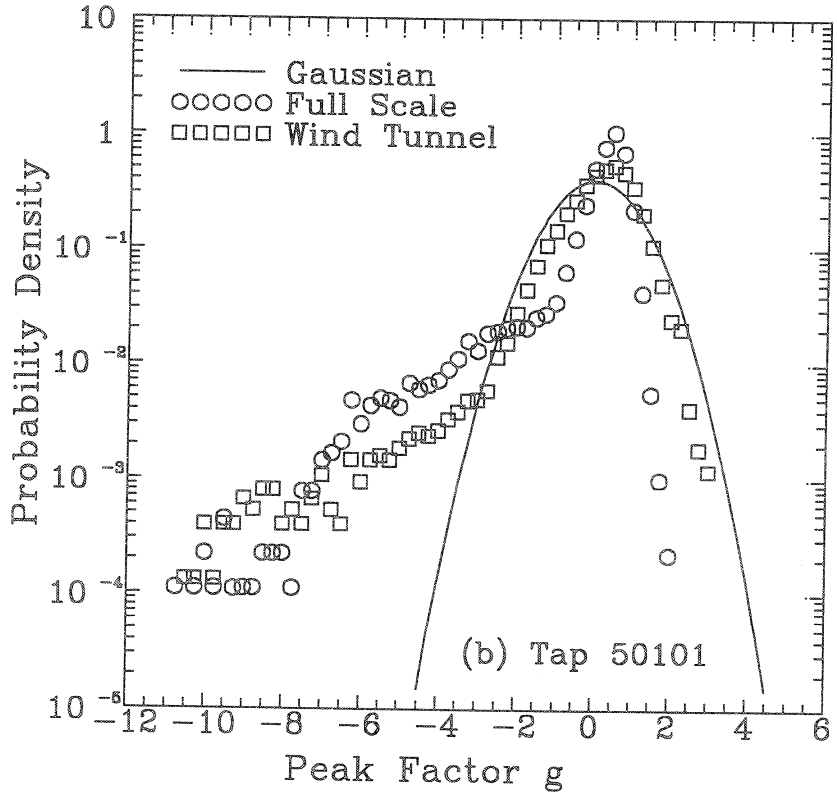

FIG.12 COMPARISON OF PROBABILITY DENSITY FUNCTIONS

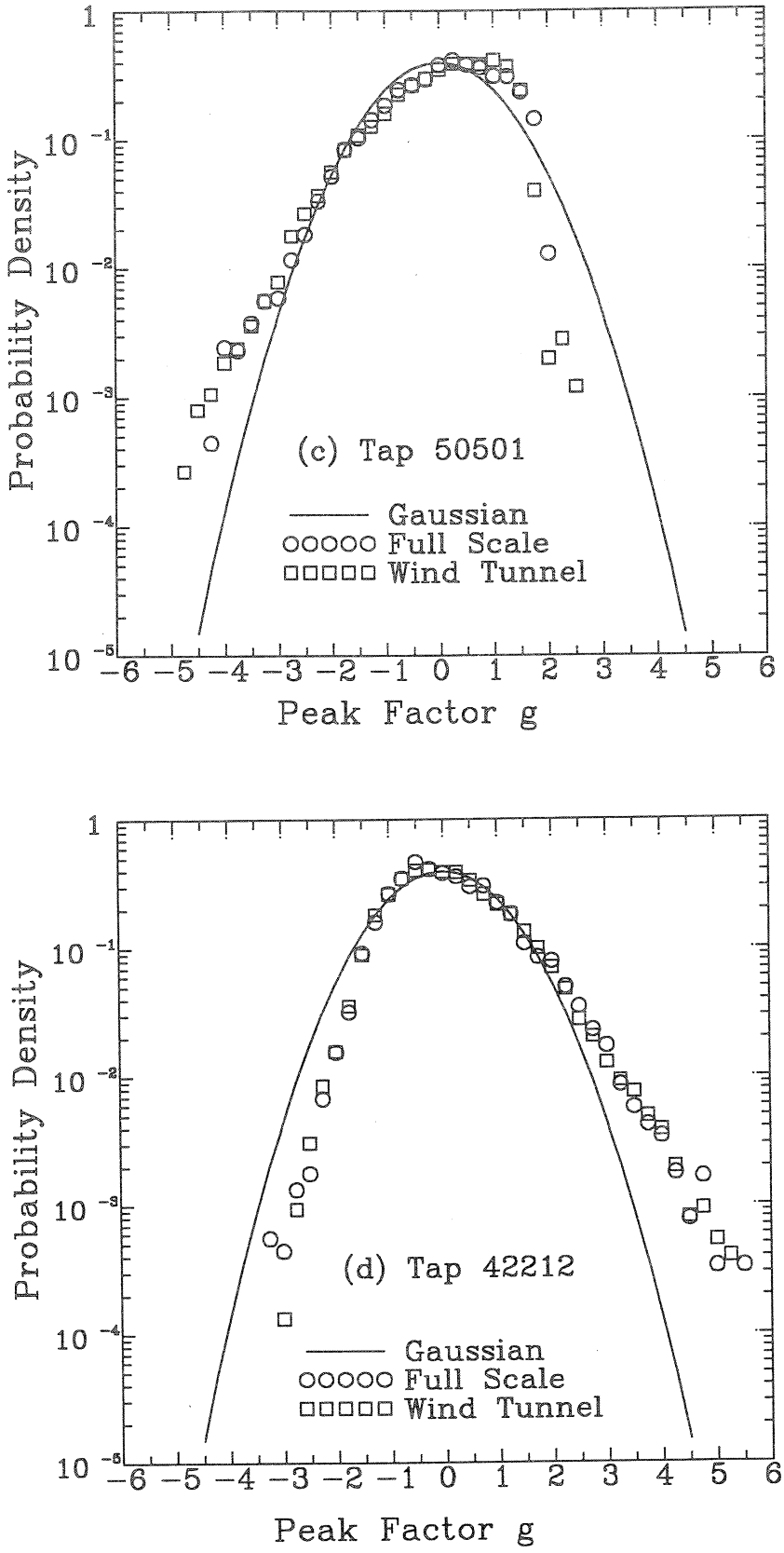

FIG.12 (continued) COMPARISON OF PROBABILITY DENSITY FUNCTIONS

leads to a reasonable agreement of load cycle distributions as shown later.

3.4 Extreme Value Distributions

Extreme value analysis of peak pressures at a particular location on a building has been used to provide a design pressure coefficient for cladding. Much research has been done in this area (e.g., Cook and Wayne, 1980; Peterka, 1983), but it is still common to simply take the single largest peak pressure from a one-hour pressure record as design pressure coefficient. Extreme value analyses of wind pressures at several critical taps were carried out in this study to decide which way should be followed to define a design pressure coefficient for fatigue loading analysis.

One-hour full-scale pressure records were provided by the Texas Tech University for taps 50101, 50501 and 50123, but for tap 42212 only one 15-minute full-scale pressure record was available for the writers. The duration of all the records from the wind tunnel tests used in the extreme value analysis were 90 seconds, which is equivalent to 75 minutes in full scale. One hundred independent largest negative peaks were selected from each record with the criterion that an independent peak has to be at least 0.05 in peak coefficient away from the adjacent valley (Peterka, 1983). A Fisher-Tippet Type (FT1) extreme value distribution was used to fit those one hundred largest independent peaks obtained from both full-scale and model-scale records.

The mode U and the dispersion 1/a of the extreme value distribution, the effective peak pressure coefficient Cp^*, the mean effective peak pressure coefficient Cp^m, and the single largest peak coefficient Cp^s are listed in Table 1 for all the concerned taps. The effective peak pressure coefficients and the mean effective peak pressure coefficients are defined as

$$C_p^* = U + \frac{1.4 + \ln(100)}{a} \tag{6}$$

$$C_p^m = U + \frac{0.577 + \ln(100)}{a} \tag{7}$$

It is noted from Table 1 that for all the roof pressures, the full-scale peak pressure coefficients are larger than the model-scale peak pressure coefficients, but for the wall pressure the model-scale peak pressure

coefficients are nearly equal to the full-scale peak pressure coefficients. These are also true for the values of the modes and dispersions. The distribution of one hundred largest peaks and the FT1 extreme value distribution used to fit the measured data are shown in Fig. 13(a) to Fig. 13(d) for taps 50123, 50101, 50501 and 42212, respectively. The reduced variate y in these figures is $a(C_p-U)$, in which C_p is one of the one hundred largest peak coefficients.

TABLE 1. RESULTS OF EXTREME VALUE ANALYSIS OF WIND PRESSURES

Tap No.	50101		50501		50123		42212	
	F.S.	M.S.	F.S.	M.S.	F.S.	M.S.	F.S.	M.S.
U	-3.65	-1.70	-6.51	-4.41	-3.27	-2.56	1.51	1.80
1/a	-0.55	-0.38	-0.49	-0.35	-0.32	-0.27	0.19	0.16
Cp^*	-6.94	-4.01	-9.45	-6.51	-5.18	-4.19	2.68	2.76
Cp^m	-6.49	-3.69	-9.05	-6.22	-4.92	-3.96	2.52	2.63
Cp^s	-7.52	-3.80	-9.00	-6.03	-4.69	-3.88	2.59	2.52
Note:F.S.=Full Scale, M.S.=Model Scale								

It is seen from these figures that the one hundred largest peak pressure coefficients from the full-scale data are larger than those from the model-scale data, but the model-scale extreme value distributions are approximately parallel to the full-scale distributions. This indicates that not only the single largest peak coefficient but also at least the next one hundred largest peak coefficients from the full-scale data are larger than those from the model-scale data, and they are somehow at approximately the same ratio.

It is also seen from these figures that for some of the taps (e.g, tap 50501) the distribution of peak pressures does fit to the FT1 distribution, but for other taps (e.g, tap 50101 in full-scale) it does not. It has been decided to use the single largest peak pressure coefficient rather than the effective peak pressure coefficient in the late fatigue loading analysis.

4 COMPARISON OF FATIGUE LOADING

The above analyses show that wind pressures on building claddings in general are broad-band non-Gaussian processes. A rainflow count method is

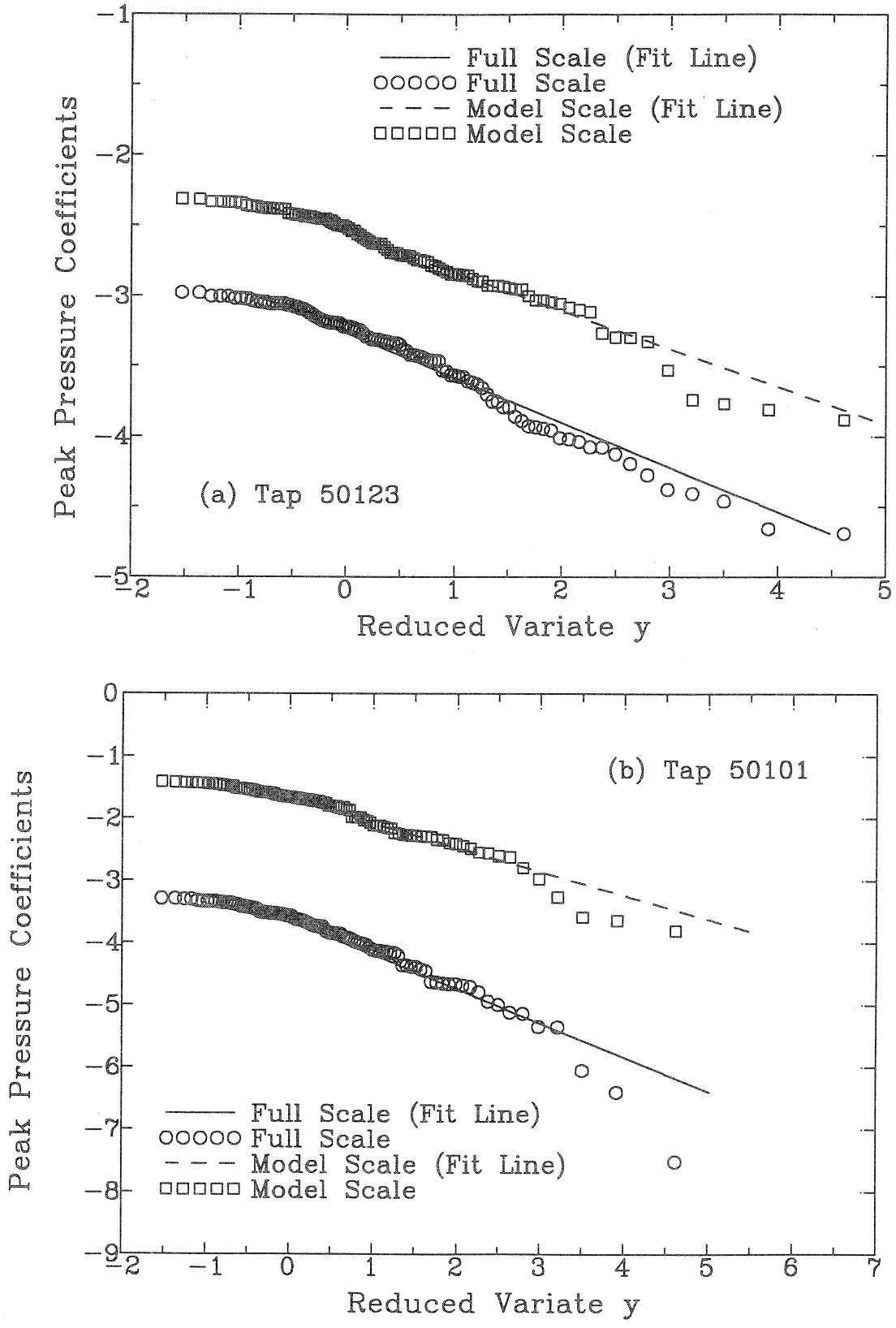

FIG.13 COMPARISON OF DISTRIBUTIONS OF ONE HUNDRED LARGEST PEAKS

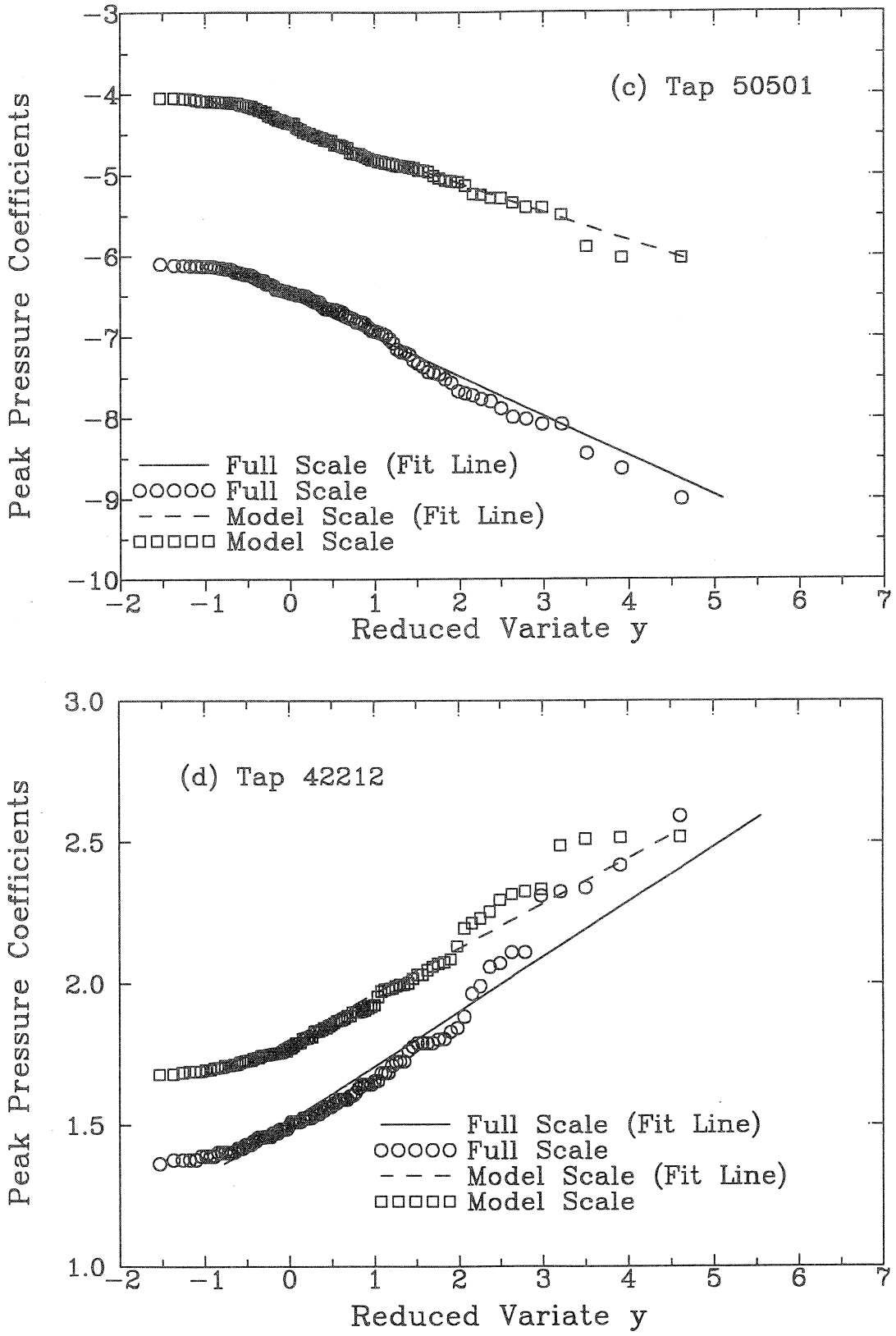

FIG.13 (continued) COMPARISON OF DISTRIBUTIONS OF ONE HUNDRED LARGEST PEAKS

therefore used to determine fatigue loading of wind pressures, characterised by the number of cycles and cycle histogram.

4.1 Rainflow Count Method

In practice, there are several equivalent definitions of the rainflow count method. The following rules for operating the rainflow count method have been described by Fuchs and Stephens (1980):

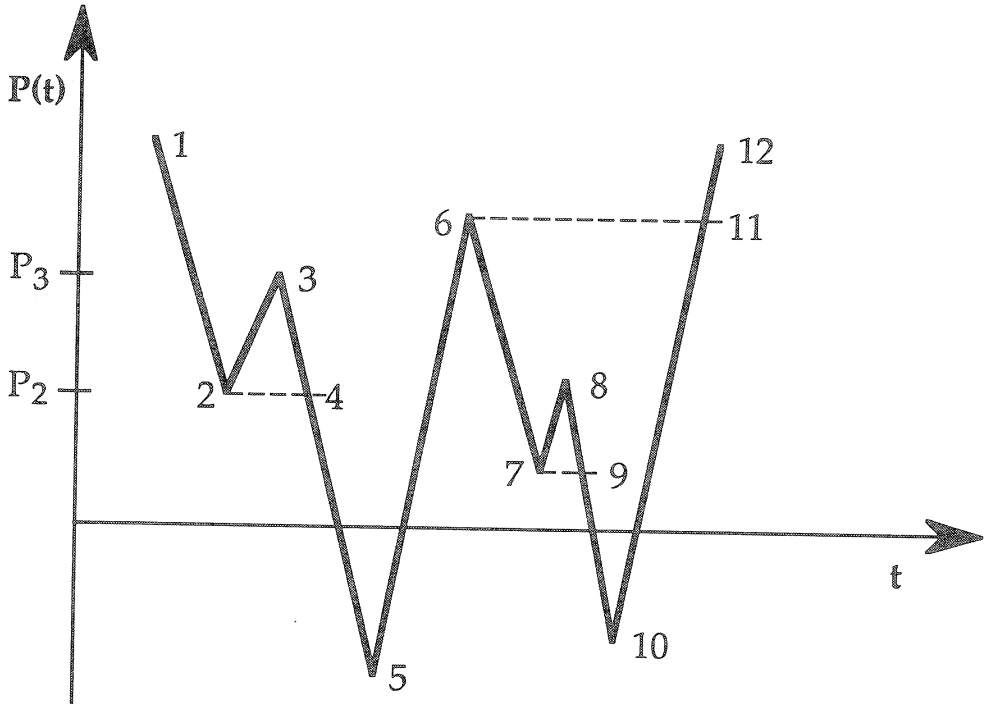

FIG.14 RAINFLOW COUNTING

1. Rearrange the history to start with the highest peak.
2. Start from the highest peak and go down to the next reversal (see Fig. 14). Proceed horizontally to the next downward range; if there is no range going down from the level of the valley at which you have stopped, go upward to the next reversal.
3. Repeat the same procedure upward instead of downward and continue these steps to the end.
4. Repeat the procedure for all the ranges and parts of a range that were not used in previous procedures.
5. If the lowest valley is more extreme than the highest peak, start with the lowest valley and go up instead of down.

By using these rules, four cycles can be identified from the sample history shown in Fig. 14. These four cycles are 1-2-4-5-6-11-12, 2-3-4, 6-7-9-10-11 and 7-8-9. The range and mean of each cycle can be determined using the coordinates of the corresponding peak and valley. For instance, the range of the cycle 2-3-4 is p_3-p_2, and the mean of the cycle is $\frac{1}{2}(p_3+p_2)$.

It is clear that the rainflow count method can identify cycles as closed hysteresis loops and provide a mean value for each cycle, and at the same time keep the original pressure history at best. A hysteresis threshold can be easily set for the size of cycle range to eliminate small cycles which contribute little to fatigue damage. The load cycles identified by the rainflow method are also compatible with a large quantity of metal roof fatigue data from constant-amplitude fatigue tests.

However, the rainflow method gives no information about original load cycle sequence, which may have a pronounced influence on the fatigue life estimation of metal roofs. Xu (1995b) discussed this issue and suggested a way to overcome this problem. It is also extremely difficult to formulate probability equations for cycle ranges and cycle means counted by the rainflow method. As a result, the rainflow method is generally used together with numerical computation.

4.2 Effects of Sampling and Cut-off Frequencies

Letchford and Norville (1994) noted that sampling frequency or cut-off frequency used in tests could affect the count of the number of cycles. The equivalent full-scale sampling frequency and cut-off frequency used in the wind tunnel tests was about 20 Hz and 2 Hz, respectively. The full-scale wind pressures were sampled at 40 Hz and low-pass filtered at 10 Hz or 8 Hz. Such differences should be taken into account so that a reasonable comparison of fatigue loading can be performed between the model scale and full scale.

To this purpose, the full-scale data were re-sampled at 20 Hz and 10 Hz and low-pass filtered at 5 Hz and 2 Hz. The digital filter was performed in the frequency domain with a cosine shaped transition from pass to no-pass. The width of the cosine shaped filter was 5% of the cut-off frequency. Corresponding to the sampling frequencies of 40, 20, and 10 Hz, the number of data points in wind pressure records was adjusted to 32768, 16384, and 8192 respectively, to maintain a record duration of 819.2 seconds in full scale. A Fortran program executing the rainflow method has been written

and used to count the number of cycles and provide cycle histogram for each record. A hysteresis threshold of 0.05 of the single largest peak coefficient was implemented when processing wind pressure records.

TABLE 2 EFFECTS OF SAMPLING FREQUENCY AND CUT-OFF FREQUENCY (TAP 50101, FULL SCALE)

Sampling Frequency (Hz)	Cut-Off Frequency (Hz)	Mean Coefficient	Rms Coefficient	Peak Coefficient	Number of Cycles
40	10	-0.603	0.389	-7.517	422
40	5	-0.603	0.381	-7.393	290
40	2	-0.603	0.363	-5.993	230
20	10	-0.603	0.389	-7.517	360
20	2	-0.603	0.364	-6.086	226
10	2	-0.603	0.368	-6.118	219

Table 2 shows the effects of sampling and cut-off frequencies on both pressure coefficient and the number of cycles at tap 50101. For a given cut-off frequency, the variation of sampling frequency does not affect the mean pressure coefficient, and only slightly affects the rms and single largest peak pressure coefficients. The variation of sampling frequency only marginally affects the number of cycles. The change of cut-off frequency also does not affect the mean pressure coefficient, and the rms pressure coefficient is only slightly reduced when cut-off frequency is reduced from 10 Hz to 2 Hz. The reduction of cut-off frequency from 10 Hz to 2 Hz however causes a change of the single largest peak pressure coefficient from -7.5 to about -6.0 and a significant reduction of the number of cycles. Since the reduction of cut-off frequency from 10 Hz to 2 Hz means the elimination of pressure fluctuation energy of higher frequency, the small-scale turbulence does affect both the single largest peak pressure coefficient and the number of cycles.

It is necessary to examine the effect of cut-off frequency or small-scale turbulence on load cycle distribution. Figs. 15 and 16 show distributions of load cycles at tap 50101. The horizontal and lateral coordinates represent the ratio of the range and mean level of cycles to the single largest peak pressure coefficient using a positive sign instead of the actual signs. the vertical axis shows the number of cycles in each cell. The number of cycles in Fig. 15 is

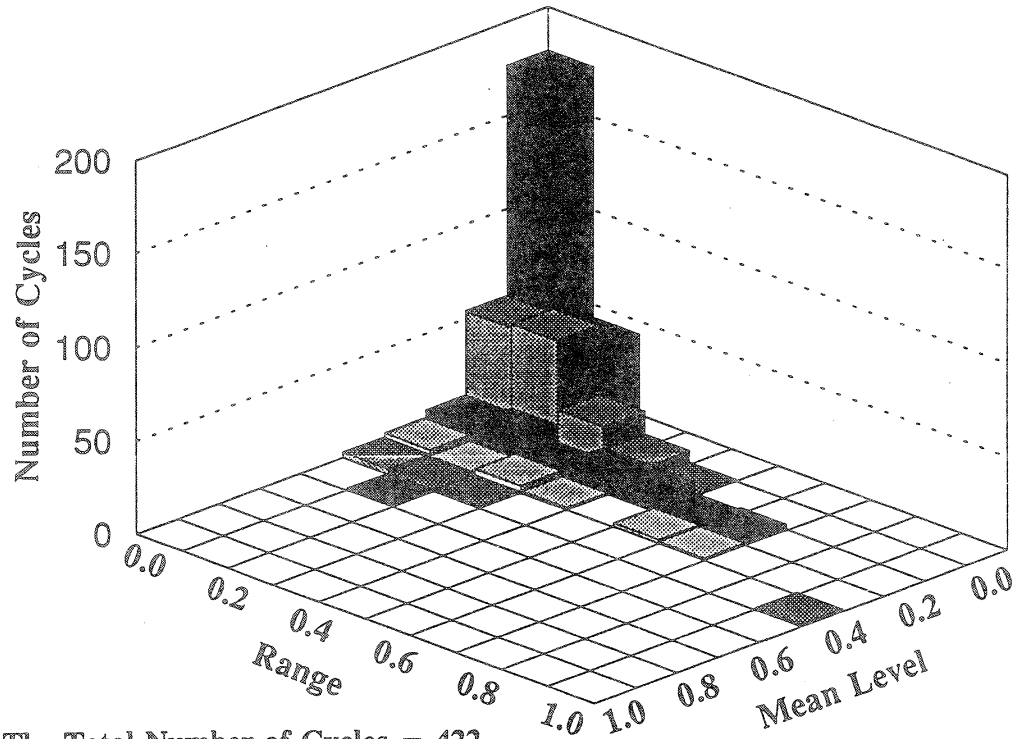

The Total Number of Cycles = 422

FIG.15 DISTRIBUTION OF LOAD CYCLES
(sampling freq. = 40 Hz; cut-off freq. = 10 Hz)

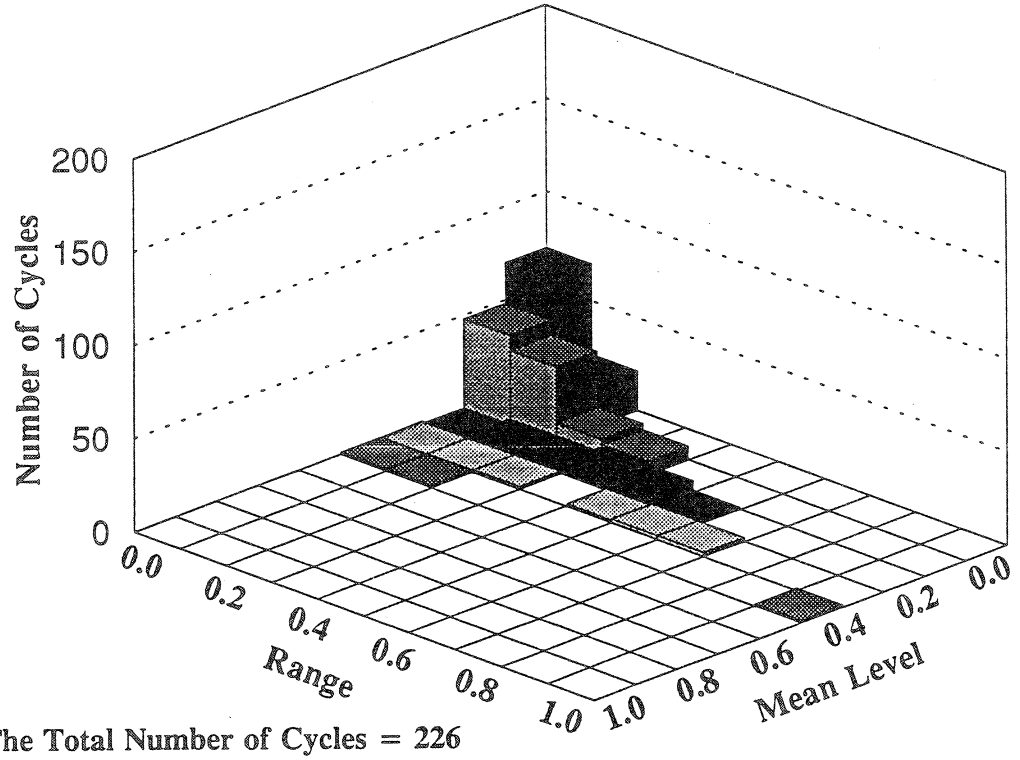

The Total Number of Cycles = 226

(b) 20 Hz Sampling Freq. and 2 Hz Cut-Off Freq.

FIG.16 DISTRIBUTION OF LOAD CYCLES
(sampling freq. = 20 Hz; cut-off freq. = 2 Hz)

obtained using a sampling frequency of 40 Hz and a cut-off frequency of 10 Hz. The number of cycles in Fig. 16 is achieved using a sampling frequency of 20 Hz and a cut-off frequency of 2 Hz. It is seen that the load cycles in Fig. 15 are different from those in Fig. 16. The significant difference of the number of cycles however is mainly in the region of both lower ranges and low cycle means. This means the cut-off of high frequency mainly affects the number of load cycles of small ranges and small means.

The same analysis was also carried out for taps 50501 and 50123. The effects of sampling and cut-off frequencies on both the number of cycles and load cycle distribution were found similar to the case of tap 50101.

4.2 The Number of Cycles in Model Scale

The model-scale wind pressure records from taps 50101, 50501, 50123 and 42212 were low-pass re-filtered at a frequency of 100 Hz equivalent to 2 Hz in full scale. The number of data points in each record was adjusted to 16384 to make a record duration of 16.4 seconds in model scale and 819.2 seconds in full scale. The results on the number of load cycles and the single largest peak coefficients are listed in Table 3 together with the full-scale results obtained using a sampling frequency of 20 Hz, a cut-off frequency of 2 Hz and a duration of 819.2 seconds.

TABLE 3. COMPARISON OF THE NUMBER OF CYCLES IN ONE RECORD

Tap No.	Scale	Mean	Rms	Peak	No.of Cycles
50101	Full Scale	-0.603	0.364	-6.086	226
	Model Scale	-0.526	0.304	-3.762	257
50501	Full Scale	-2.312	1.074	-8.261	503
	Model Scale	-1.472	0.856	-5.131	410
50123	Full Scale	-1.056	0.382	-3.641	451
	Model Scale	-1.078	0.399	-3.066	371
42212	Full Scale	-0.614	0.362	2.361	502
	Model Scale	-0.642	0.346	2.246	517

If considering the similarity equation of the Strouhal Number, one would expect that the number of load cycles in full scale and model scale should

approximately satisfy the following equation.

$$\frac{N_p}{U_{rp}t_p} = \frac{N_m}{U_{rm}t_m}\frac{L_m}{L_p} \tag{8}$$

where N = the number of cycles; L = the geometric length; t = the time; and the indices p and m stand for prototype and model, respectively.

The reference velocity used in the model tests was nearly the same as the full-scale reference velocity. The record duration divided by the length ratio was the same in both full-scale and model-scale tests. The numbers of cycles listed in Table 3 from the wind tunnel tests are therefore expected to be approximately the same as those from the full-scale tests. It is encouraging to see that the number of cycles at the wall pressure tap 42212 from the wind tunnel test is in good agreement with the full-scale result. The numbers of cycles at taps 50123 and 50501 from the model tests are less than those from the full-scale tests whilst the number of cycles at tap 50101 is slightly larger in the model-scale data than in the full-scale data.

Because the wind pressures concerned here were broad band and some uncertainties were involved in both the model-scale and full-scale tests (such as the simulation of small-scale turbulence and Reyholds number in the wind tunnel and the variation of wind direction in the field), it is believed that the numbers of cycles obtained from both the model- and full-scale tests are in reasonable agreement. This reasonable agreement could be improved if the uncertainties mentioned above are resolved and the average values from several pressure records rather than one record are used. The important point is that the sampling frequency, the sampling duration, and particularly the cut-off frequency used in the model tests must be equivalent to those used in the full-scale tests.

It is also noted from Table 3 that the number of cycles at tap 50501 is close to that at tap 42212 though their single largest peak pressure coefficients are significantly different. The number of cycles at tap 50101 however is much lower than other taps. The difference in the number of cycles can cause a significant difference of the total fatigue loading when considering long-term wind climate effects (Xu, 1995a). Further research should be done to investigate the variation of fatigue loading with tap location on a building.

4.3 Cycle Histograms

The rainflow count method can provide a three dimensional cycle histogram, showing load cycle distribution over both cycle ranges and cycle means. The cycle histogram, the number of cycles and the single largest peak coefficient can then be used to determine final total fatigue loading on claddings together with information on wind climate (Xu, 1995a). Figs. 17(a) to 17(d) display the cycle histograms for each of the four concerned taps using the wind tunnel test results. The vertical axis shows the proportion of the number of cycles in each cell to the total number of cycles summed from all cells. The horizontal and lateral coordinates represent the ratio of the range and mean of cycles to the single largest peak coefficient.

It is seen that the cycle histogram for tap 50501 is similar to that for tap 42212. This is consistent with the comparability of the probability density functions of the two taps. These two histograms however are significantly different from the cycle histogram of tap 50101. The load cycles of tap 50101 are more concentrated on the region of both lower cycle ranges and cycle means. There are only a few cycles in higher cycle ranges. Compared with other taps, the load cycles of tap 50501 is most uniformly distributed and therefore there are more cycles in higher cycle ranges. These features are compatible with the probability density functions described in Section 3.2. More research however is required to find the relationship between the probability density function and the load cycle histogram and, if possible, the mathematical models of cycle histograms.

The cycle histograms obtained using full-scale data are shown in Figs. 18(a) to 18(d). The pressure records used are of a 819.2 seconds duration, a 20 Hz sampling frequency and a 2 Hz cut-off frequency, being the same as used in the above analysis of the model-scale data. The full-scale cycle histograms of taps 50501 and 42212 are similar to the corresponding model-scale cycle histograms. Taps 50123 and 50101 however exist some differences between the full- and model-scale cycle histograms, but the basic characteristics still remain. This similarity of the cycle histograms and the number of cycles between the model- and full-scale tests indicates that wind tunnel pressure tests can be used to determine fatigue characteristics of wind pressures on buildings if the sampling parameters are appropriately selected and the currently-used simulation technique is improved. The improved simulation technique is also expected to solve the difference of the largest peak coefficients between the model- and full-scale results.

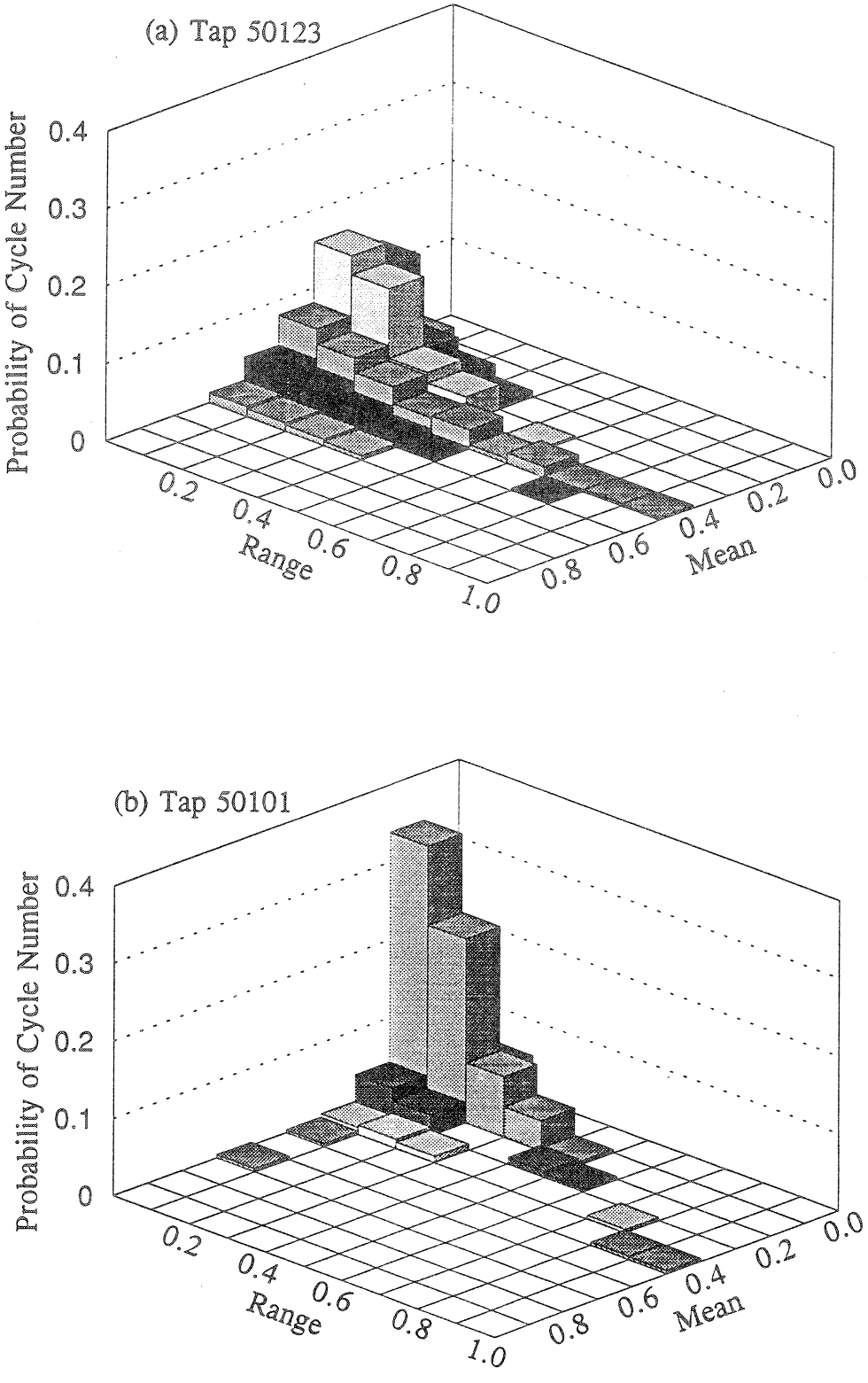

FIG.17 CYCLE HISTOGRAMS OF WIND PRESSURES (MODEL SCALE)

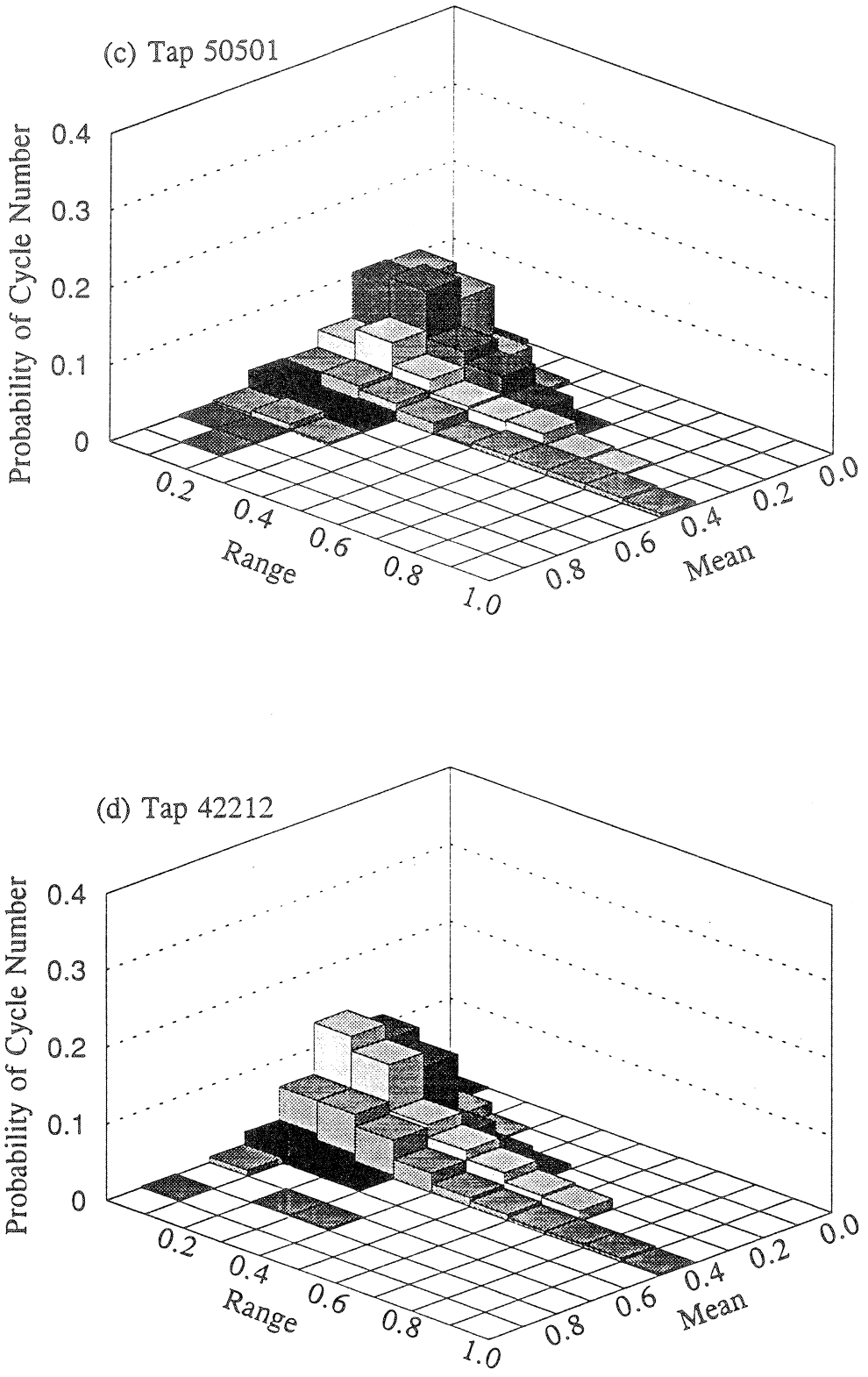

FIG.17 (continued) CYCLE HISTOGRAMS OF WIND PRESSURES (MODEL SCALE)

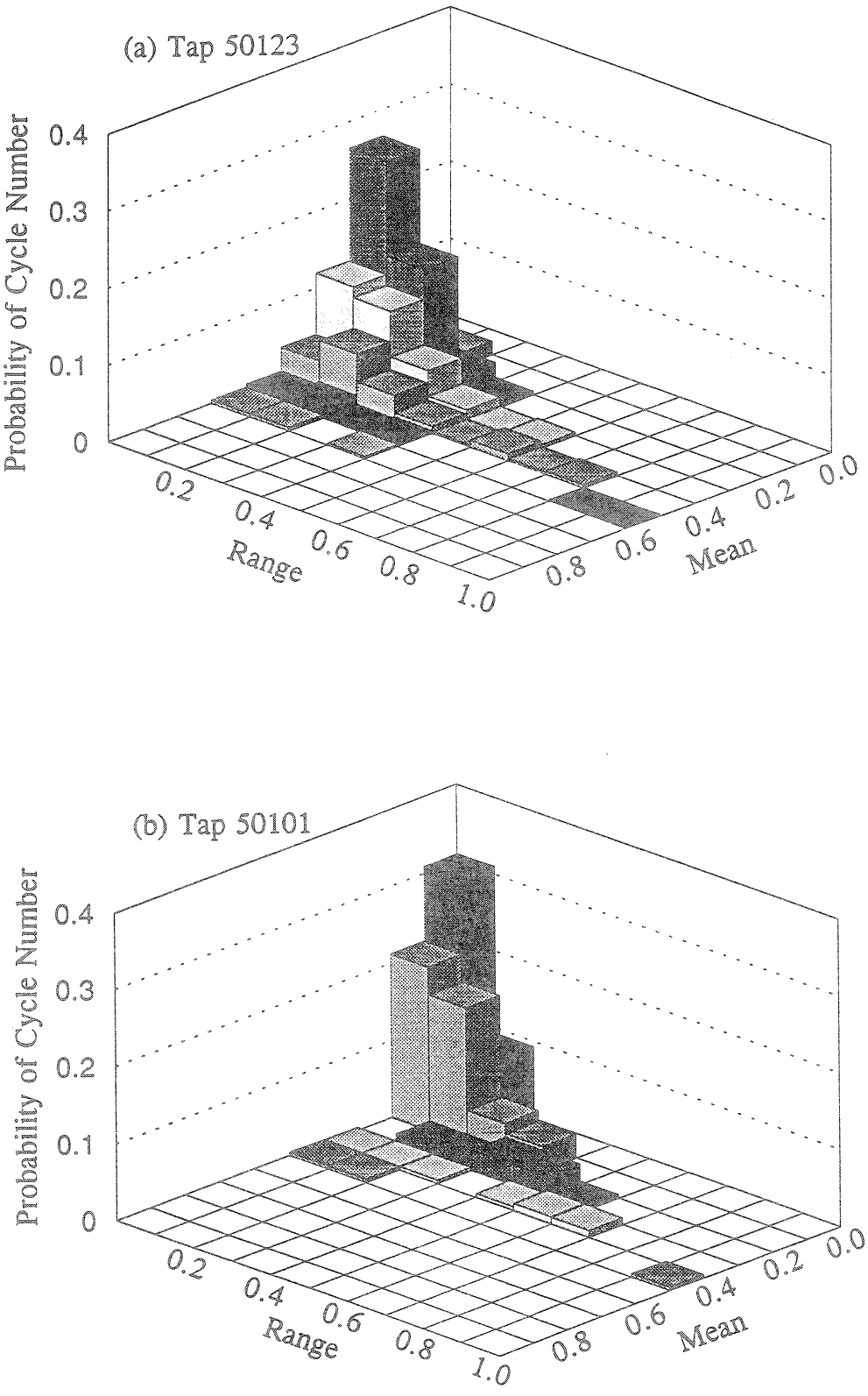

FIG.18 CYCLE HISTOGRAMS OF WIND PRESSURES (FULL SCALE)

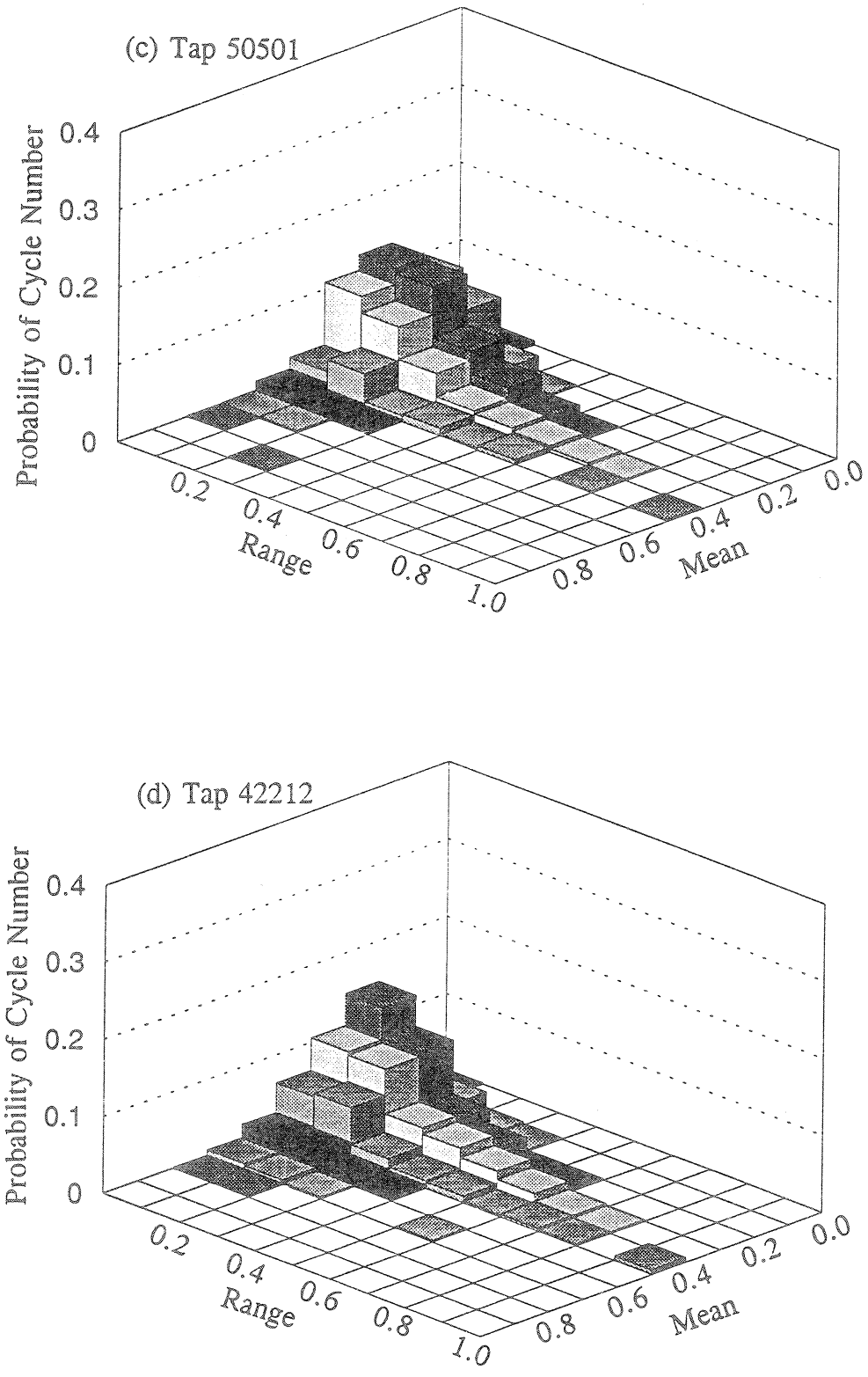

FIG.18 (continued) CYCLE HISTOGRAMS OF WIND PRESSURES (FULL SCALE)

5 CONCLUSIONS

A model-scale and full-scale comparison of wind pressures and fatigue loading on the Texas Tech University Building has been carried out at the James Cook Cyclone Testing Station. Most wind pressure coefficients measured on the model were in close agreement with full-scale pressure coefficients, but the largest negative peak coefficients at the roof edge and roof corners were underestimated by the wind tunnel tests. The consistency and disparity of the full-scale and model-scale data also appeared in wind pressure spectra, probability distributions and extreme value distributions of wind pressures.

The rainflow count method was used to obtain the number of cycles and cycle histograms since the wind pressures concerned here were broad-band non-Gaussian processes. It was found that there was a good agreement of the number of cycles and cycle histogram for the wall pressure and a reasonable agreement for the roof pressures when the sampling frequency, the sampling duration, and particularly the cut-off frequency used in the model tests were equivalent to those used in the full-scale tests. The agreement of fatigue loading was compatible with the comparison of stochastic characteristics of wind pressures. It was also found that the number of cycles and cycle histogram varied with tap location on the building. The most severe fatigue loading was on tap 50501, located at the roof corner of the building.

In summary, wind tunnel techniques can be used as an economic and efficient way to determine wind pressures and fatigue loading on low-rise buildings, but caution should be given to the largest negative peak pressures at roof edge and roof corners.

6 ACKNOWLEDGMENTS

This research project is partly supported by a Merit Research Grant from James Cook University (JCU) of North Queensland, to which the writers are grateful. They wish to thank Dr Holmes, Chief Research Scientist of CSIRO, for his valuable comments regarding wind tunnel tests. Thanks are also due to Professor Mehta and Mr Yeatts at the Texas Tech University for making the full-scale data available, and Mr McNealy, Senior Technical Officer at JCU for carrying out most of the wind tunnel tests described here.

7 REFERENCES

Cermak, J.E. and Cochran, L.S. (1992) "Physical modelling of the atmospheric surface layer", J. of Wind Eng. and Ind. Aerodyn., 41-44, pp.935-946.

Cochran, L.S. and Cermak, J.E. (1992) "Full- and model-scale cladding pressures on the Texas Tech University Experimental Building", J. of Wind Eng. and Ind. Aerodyn., 41-44, pp. 1589-1600.

Cook, N.J. and Mayne, J.R. (1980) "A refined working approach to the assessment of wind loads for equivalent static design", J. of Wind Eng. and Ind. Aerodyn., 6, pp. 125-137.

Holmes, J.D. (1980) "Wind Pressures and Forces on Tropical Houses", Final Report of Project No.17 of the Australian Housing Research Council.

Letchford, C.W. and Norville, H.S. (1994) "Wind pressure loading cycles for glazing during hurricanes", Proc. of the Second Int. Workshop on Full Scale Behaviour of Low Rise Buildings, Townsville, Australia.

Levitan, M.L. and Mehta, K.C. (1992a) "Texas Tech field experiments for wind loads, part 1 : building and pressure measuring systems", J. of Wind Eng. and Ind. Aerodyn., 41-44, pp. 1565-1576.

Levitan, M.L. and Mehta, K.C. (1992b) "Texas Tech field experiments for wind loads, part 2 : meteorological instrumentation and terrain", J. of Wind Eng. and Ind. Aerodyn., 41-44, pp. 1577-1588.

Mehta, K.C., Levitan, M.L., Iverson, R.E. and McDonald, J.R. (1992) "Roof pressures measured in the field on a low building", J. of Wind Eng. and Ind. Aerodyn., 41-44, pp.182-192.

Peterka, J.A. (1983) "Selection of local peak pressure coefficients for wind tunnel studies of buildings", J. of Wind Eng. and Ind. Aerodyn., 13, pp. 477-488.

Peterka, J.A. and Cermak, J.E. (1975) "Wind pressure on buildings - probability densities", J. of Struct. Div., ASCE, Vol. 101, No. ST6, pp.1255-1267.

SAA (1989) "AS1170.2 - SAA loading code, part 2: wind loads", Standard Association of Australia.

Smith,T.L. (1993) "Causes of roof damage and roof failure modes: insights provided by Hurricane Andrew", Proc. of Symposium on Hurricanes of 1992, ASCE, Miami, USA.

Stathopoulos, T. (1982) "PDF of wind pressures on low-rise buildings", J. of Struct. Div., ASCE, Vol. 106, No. ST5, pp. 973-990.

Stathopoulos, T. (1984) "Wind loads on low-rise buildings: a review of the state of the art", Eng. Struct., Vol.6, pp. 119-135.

Surry, D. (1991) "Pressure measurements on the Texas Tech Building: wind tunnel measurements and comparisons with full-scale", J. of Wind Eng. and Ind. Aerodyn., 38, pp.235-247.

Tieleman, H.W. (1993) "Wind loads on roofs of low rise structures: buffeting or interaction", Proc. of Symposium on Hurricanes of 1992, ASCE, Miami, USA.

Walker, G.R. (1975) "Report on Cyclone Tracy - Effect on Buildings - December 1974", Vol. 1, Australian Department of Housing and Construction.

Xu, Y.L. (1995a) "Determination of wind-induced fatigue loading on roof cladding", J. of Eng. Mech., ASCE (in print).

Xu, Y.L. (1995b) "Fatigue performance of screw-fastened light gauge steel roofing sheets", J. of Struct. Eng., ASCE (in print).

Yeatts, B.B. and Mehta, K.C. (1993) "Field experiments for building aerodynamics", J. of Wind Eng. and Ind. Aerodyn., 50, pp. 213-224.